Modeling the Diurnal Variability of Agricultural Ammonia in Bakersfield, California during the CalNex Campaign

C. R. Lonsdale[1], J. D. Hegarty[1], K. E. Cady-Pereira[1], M. J. Alvarado[1], D. K. Henze[2], M. D. Turner[2], S. L. Capps[2], J. B. Nowak[3,4,*], J. A. Neuman[4], A. M. Middlebrook[4], R. Bahreini[4], J. G. Murphy[5], M. Z. Markovic[5**], T. C. VandenBoer[5***], L. M. Russell[6], A. J. Scarino[7]

[1]Atmospheric and Environmental Research, Lexington, MA, USA
[2]Department of Mechanical Engineering, University of Colorado, Boulder, CO, USA
[3]Cooperative Institute for Research in Environmental Sciences, University of Colorado Boulder, CO, USA
[4]Chemical Sciences Division, Earth System Research Lab, NOAA, Boulder, CO, USA
[5]Department of Chemistry, University of Toronto, Toronto, ON Canada
[6]Scripps Institution of Oceanography, University of California, San Diego, CA, USA
[7]Science Systems and Applications Inc., Hampton, VA, USA
*Now at Aerodyne Research, Inc. Billerica, MA, USA
**Now at Picarro, Inc., Santa Clara, CA, USA
*** Now at Department of Earth Sciences, Memorial University of Newfoundland, NL Canada

Correspondence to: C. R. Lonsdale (clonsdal@aer.com)

Abstract. NH_3 retrievals from the NASA Tropospheric Emission Spectrometer (TES), as well as surface and aircraft observations of $NH_{3(g)}$ and submicron $NH_{4(p)}$, are used to evaluate modelled concentrations of $NH_{3(g)}$ and $NH_{4(p)}$ from the Community Multiscale Air Quality (CMAQ) model in the San Joaquin Valley (SJV) during the California Research at the Nexus of Air Quality and Climate Change (CalNex) campaign. We find that simulations of NH_3 driven with the California Air Resources Board (CARB) emission inventory are qualitatively and spatially consistent with TES satellite observations, with a correlation coefficient (r^2) of 0.64. However, the surface observations at Bakersfield indicate a diurnal cycle in the model bias, with CMAQ overestimating surface NH_3 at night and underestimating it during the day. The surface, satellite, and aircraft observations all suggest that daytime NH_3 emissions in the CARB inventory are underestimated by at least a factor of two, while the night-time overestimate of $NH_{3(g)}$ is likely due to a combination of overestimated NH_3 emissions and underestimated deposition.

Running CMAQ v5.0.2 with the bi-directional NH_3 scheme reduces NH_3 concentrations at night and increases them during the day. This reduces the model bias when compared to the surface and satellite observations, but the increased concentrations aloft significantly increase the bias relative to the aircraft observations. We attempt to further improve the model by using the surface observations at Bakersfield to derive an empirical diurnal cycle of NH_3 emissions in the SJV, in which night-time and midday emissions differ by about a factor of 4.5. Running CMAQv5.0.2 with a bi-directional NH_3 scheme as well as this emissions diurnal profile further reduces model bias relative to the surface observations. Comparison of these simulations with the vertical profile retrieved by TES shows little bias except for the lowest retrieved level, but the

model bias relative to flight data aloft increases slightly. Our results indicate that both diurnally-varying emissions and a bi-directional NH_3 scheme should be applied when modelling $NH_{3(g)}$ and $NH_{4(p)}$ in this region. The remaining model errors suggest that the bi-directional NH_3 scheme in CMAQ v5.0.2 needs further improvements to shift the peak NH_3 land-atmosphere flux to earlier in the day. We recommend that future work include: updates to the current CARB NH_3 inventory to account for NH_3 from fertilizer, livestock, and other farming practices separately; adding revised information on crop management practices specific to the SJV region to the bi-directional NH_3 scheme; and top-down studies focused on determining the diurnally-varying biases in the canopy compensation point that determines the net land-atmosphere NH_3 fluxes.

1 Introduction

The emissions of ammonia (NH_3) to the atmosphere are highly uncertain (e.g., Pinder et al., 2006; Beusen et al., 2008; Galloway et al., 2008; Henze et al., 2009; Schlesinger, 2009). Nitrogen dioxide (NO_x = NO + NO_2) and sulfur dioxide (SO_2) photo-oxidize in the atmosphere to form nitric acid (HNO_3) and sulfuric acid (H_2SO_4), respectively, which react with atmospheric gas-phase ammonia ($NH_{3(g)}$) to form ammonium sulfate ($(NH_4)_2SO_4$) and ammonium nitrate (NH_4NO_3) aerosol. Uncertainty in NH_3 emissions therefore leads to significant uncertainties in the concentrations of secondary inorganic aerosols. Ammonium sulfate and nitrate aerosols contribute to fine particulate matter concentrations ($PM_{2.5}$), and thus to decreased visibility, altered climate, and acidification and eutrophication in sensitive ecosystems (e.g., Paulot et al., 2014; RoTAP. 2012; Bricker et al., 2007; Martin et al., 2004).

$PM_{2.5}$ also causes adverse health effects (WHO, 2016; Pope et al., 2004). In particular, some regions in the San Joaquin Valley (SJV) in California have been designated as non-attainment areas for $PM_{2.5}$, with NH_3 emissions contributing to more than half of the inorganic $PM_{2.5}$ in the state (Schiferl et al., 2014), depending on ambient conditions and concentrations (Lonsdale et al., 2012). During the NOAA California Research at the Nexus of Air Quality and Climate Change (CalNex) campaign in May and June of 2010, however, concentrations of $PM_{2.5}$ rarely exceeded the National Ambient Air Quality Standard (NAAQS) in the SJV, as $PM_{2.5}$ exceedances here generally happen in the winter. While emissions of NO_x and SO_2 are relatively well constrained, are regulated by the United States Environmental Protection Agency (US EPA), and are predicted to continually decrease due to air quality regulations and emission reducing technologies (US EPA, 2010), NH_3 emissions are not currently regulated and are predicted to stay constant or increase over the next several decades in the US due to an increasing population and associated increases in farming and agricultural activities (Moss et al., 2010). Climate change is also predicted to increase NH_3 emissions (+0-40 % in north-central Europe) with larger countries having the largest uncertainty in emissions variations (Skjøth et al., 2013).

Anthropogenic NH_3 sources in the SJV are dominated by agricultural activities, with livestock waste estimated to contribute about 74 % of total anthropogenic NH_3 to the atmosphere and chemical fertilizer use another 16 % (Simon et al., 2008). Agricultural emissions of NH_3 can be highly variable due to factors such as the differences in fertilizer application, the diet

provided to livestock, and waste management and storage practices of farmers (Hristov et al., 2011; Sawycky et al., 2014). In addition, while $NH_{3(g)}$ can be quickly deposited to the surface causing soil acidification, water eutrophication, and an imbalance of ecosystems when in excess (e.g., Carfrae et al., 2004), the air-surface exchange of NH_3 is bi-directional, with the direction of the NH_3 flux between the land and the atmosphere varying with temperature, relative humidity, vegetation and soil type, maintenance (e.g., cutting and tilling practices), and fertilizer applications (Nemitz et al., 2001; Zhang et al., 2010; Ellis et al., 2011; Bash et al., 2013; Sawycky et al., 2014). This complexity in the emission and deposition of NH_3, along with the rapid reactions of NH_3 with HNO_3 and H_2SO_4 and the consequently short (~1 day) atmospheric lifetime of NH_3, leads to large temporal and spatial variability of this gas, as seen in in situ measurements (e.g., Langford et al., 1992; Carmichael et al., 2003; Nowak et al., 2010; Walker et al., 2013) and in satellite retrievals (e.g., Clarisse et al., 2013; Pinder et al., 2011; Shephard et al., 2011; Heald et al., 2012; Sun et al., 2015; Shephard and Cady-Pereira, 2015; Shephard et al., 2015).

Recent studies have recognized a diurnal pattern of NH_3 emissions from livestock attributed to potential differences in farm management practices, livestock housing outflow patterns, and variations in soil moisture, temperature, and wind speed (Hensen et al., 2009; Zhu et al., 2015a; Zhu et al., 2015b). To account for this, a diurnal variability scheme was implemented into global simulations using the global 3-dimensional chemical transport model, GEOS-Chem, and was shown to decrease NH_3 concentrations globally (Zhu et al., 2015a). That study also calculated the bi-directional exchange of NH_3, which decreased NH_3 concentrations in the US in the months of October through April and increased it in the month of July (Zhu et al., 2015a). Bash et al. (2013) also explored the sensitivity of modelled NH_3 concentrations to a bi-directional NH_3 scheme that used meteorological factors, including temperature, wind speed, agricultural crop flux values, and a nitrogen soil geochemistry parameterization in the CMAQ model. They found that over the continental US their model run with the bi-directional NH_3 scheme decreased the total dry deposition of NH_3 by 45 %, thus increasing atmospheric NH_3 concentrations and NH_x wet deposition by 10 % and 14 %, respectively. Wichink Kruit et al. (2012) use the DEPosition of Acidifying Compounds (DEPAC) surface-atmospheric exchange module in a CTM and saw an increase in atmospheric NH_3 almost everywhere in their model domain, including decreased NH_3 deposition with a remaining underestimation in agricultural areas.

Previous studies have also shown that errors in NH_3 emissions are a common contributing factor to modelled $PM_{2.5}$ and NH_3 bias (e.g., Schiferl et al., 2014). Skjøth et al., (2011) discuss their method for calculating dynamic NH_3 emissions that includes distributions of agricultural NH_3 in Europe. Their method is designed for use in chemical transport models and their results show considerable improvements made in the agricultural NH_3 sector, particularly in areas with detailed records of agricultural practices. Inverse modelling studies have been used to reduce the uncertainty in NH_3 emissions as well, generally by assimilating surface observations of the wet deposition of ammonium (NH_4^+) in precipitation. Gilliland et al. (2003) used the CMAQ model to determine that the 1990 version of the US EPA National Emissions Inventory (NEI) overestimated total emissions of NH_3 by 20 %. Gilliland et al. (2006) performed a similar study for the 2001 NEI and found that total emissions of NH_3 were represented well, but needed to be increased in summer and reduced in winter. Henze et al.

(2009) used the adjoint of the global chemical transport model GEOS-Chem to assimilate the Inter Agency Monitoring of Protected Visual Environments (IMPROVE) observations and found that total US NH_3 emissions for 1998 were overestimated.

More recently, satellite observations of NH_3 have been incorporated into inverse studies. By assimilating satellite retrievals of NH_3 concentrations from the Tropospheric Emission Spectrometer (TES) (Beer et al., 2008; Shephard et al., 2011) aboard the NASA Aura satellite, it has been found that NH_3 emission sources in GEOS-Chem are broadly underestimated (Zhu et al., 2013). Heald et al. (2012) and Walker et al. (2012) used IMPROVE data and satellite retrievals of NH_3 from the Infrared Atmospheric Sounding Instrument (IASI, Van Damme et al., 2014) to show that NH_3 emissions are likely underestimated in GEOS-Chem for California, leading to a local underestimate of $NH_{4(p)}$. Other infrared nadir sounders have been used to provide satellite observations of NH_3. For example, Shephard and Cady-Pereira (2015) demonstrated the ability of the Crosstrack Infrared Sounder (CrIS) aboard the joint NOAA-NASA Suomi National Polar-orbiting satellite to measure daily, spatially distributed tropospheric NH_3 in California, and in preliminary results found it correlated well with Deriving Information on Surface Conditions from Column and Vertically Resolved Observations Relevant to Air Quality (DISCOVER-AQ) measurements in the SJV in January 2013.

Investigating the formation, transport, and fate of $NH_{3(g)}$ and $NH_{4(p)}$ in California was one of the major goals of the CalNex field campaign, which provided measurements from flights and surface sites (Ryerson et al., 2012). Nowak et al. (2012) used this data to demonstrate the importance of ammonium nitrate formation downwind of the Los Angeles urban core and dairy facilities further east. They found that NH_3 emissions from these dairy farms were underestimated by a factor of 3 or more, thus indicating the need for better representation in this emission sector. Kelly et al. (2014) in general saw well-correlated comparisons of CMAQ model estimates to measurements from the EPA's Chemical Speciation Network. Their model tended to under-predict NH_x ($NH_x = NH_{3(g)} + NH_{4(p)}$) during the day at the Bakersfield, CA site and significantly over-predict $NH_{3(g)}$ at night. They suggest that this model bias may be due to emissions from livestock and dairy farms being too low and lacking in variability in this region or to errors in crustal cation predictions and the missing effects of organic acids and amines on inorganic aerosol thermodynamics (Kelly et al., 2014).

Model estimates of the planetary boundary layer (PBL) height are essential in correctly quantifying changes in atmospheric pollutant concentrations, especially for short-lived pollutants like NH_3. Such estimates are difficult at fine spatial and temporal scales, especially in the complex terrain of the SJV. Scarino et al. (2014) studied the PBL and mixed layer heights during CalNex using WRF and high spectral resolution lidar (HSRL) data taken during the campaign. They found that, in general, there is good agreement between the WRF modelled output and measured values; however, in the California Central Valley there is a WRF mixed-layer height over-prediction and an inability to represent the diurnal growth of the mixed layer in the early part of the day. Additionally they suggest that future improvements will require a focus on mixing layer characteristics, soil moisture, and temperature. Baker et al. (2013) explored how well the WRF model configuration used to drive the CMAQ simulations of Kelly et al. (2014) simulates PBL height during CalNex, using two versions of WRF. The study shows that both WRF versions simulate the PBL and mixing layers well within the SJV, as well as other large scale

flow patterns, but under-predict local wind speed and temperature. A strong aerosol gradient is used to identify the top of the PBL in HSRL measurements, which may also be present in a night-time residual layer. Baker et al. (2013) take this into account by identifying the surface-attached mixed layer, which they assume as the lowest significant gradient in such a circumstance.

In this study, we use the CalNex observations of $NH_{3(g)}$ and $NH_{4(p)}$ and the CMAQ model to evaluate the estimates of NH_3 emissions in the SJV contained in the California Air Resources Board (CARB) inventory (Figure 1). While previous NH_3 model evaluation efforts using CalNex data have focused on the NEI inventory (Kelly et al., 2014; Heald et al., 2012; Walker et al., 2012), the CARB inventory is used in the development of California's State Implementation Plans (SIPs) under the Clean Air Act, and so ensuring the accuracy of this emission inventory is important to the design of air quality policy for the SJV and California in general. In addition, previous studies have not taken advantage of the high-resolution observations of $NH_{3(g)}$ made by the TES satellite instrument over Bakersfield during the CalNex campaign. Here we evaluate the consistency of the satellite, aircraft, and surface observations of $NH_{3(g)}$ and $NH_{4(p)}$ during the CalNex campaign and then use these observations, along with lidar retrievals of PBL height, to investigate the biases in the magnitude and diurnal cycle of emissions of $NH_{3(g)}$ from the CARB inventory in the SJV. We also explore the sensitivity of modelled NH_3 concentrations to bi-directional NH_3 exchange using the bi-directional NH_3 flux scheme in CMAQv5.0.2.

Section 2 briefly describes the data sources used in this study, while Section 3 describes the CARB emission inventory and the configurations used for the WRF, the Hybrid Single-Particle Lagrangian Integrated Trajectory (HYSPLIT), and CMAQ model runs. The performance of the CARB inventory used in our CMAQ simulations, along with model sensitivity studies, is presented in Section 4. Section 5 discusses the remaining errors in our final model configuration in detail and makes suggestions for further model improvements, while our conclusions are discussed in Section 6.

2 Data

2.1 NOAA WP-3 aircraft

The NOAA WP-3 aircraft completed 18 research flights during the CalNex campaign, which included measurements of $NH_{3(g)}$ and $NH_{4(p)}$. $NH_{3(g)}$ was measured at 1 s (~100 m) intervals using chemical ionization mass spectrometry (CIMS) with an uncertainty of +/- 30 % as described in detail in Nowak et al. (2007). The CIMS instrument sampled air through a 0.55 m long heated teflon inlet with a fast flow. Measurement artifacts were accounted for by quantifying and subtracting the background signal originating from NH_3 desorption from instrument surfaces. The background signal was determined in flight by actuating a teflon valve at the inlet tip once every half hour to divert the sample air through a scrubber that removes NH_3 from the ambient air stream (Nowak et al, 2007). Additionally, standard addition calibrations from a NH_3 permeation tube were performed several times each flight to determine instrument sensitivity. Submicron $NH_{4(p)}$ was measured at 10 s (~ 1 km) intervals with an uncertainty of ~ 30 % using a compact time-of-flight aerosol mass spectrometer from Aerodyne (c-TOF AMS, Bahreini et al., 2009). In this study we focused on the flights of 24 of May and 16 and 18 of June when the WP-3

was sampling air in the SJV (Figure 1). The quality-controlled flight data were reported at a merged time resolution of 1 s, which we averaged to 1 minute values (the approximate time it takes the WP-3 to cross a 4 km CMAQ grid box) and then matched the sample times and locations to the corresponding time and location of the CMAQ hourly concentration output.

2.2 Bakersfield surface observations

Bakersfield, California is located on the southern part of the SJV (35.35°N, 118.97°W, 20 m asl) and there is a general north-to-south orographic air-flow in this region, with a tendency for emissions to get trapped in the valley due to the nearby mountains (Baker et al., 2013). At the Bakersfield ground site the Ambient Ion Monitor Ion Chromatograph (AIM-IC, Ellis et al., 2010, Markovic et al., 2012) was used to measure $NH_{3(g)}$ on an hourly basis, with an uncertainty of +/- 20 % and a detection limit of 41 ppt. The sampling inlet for the AIM-IC consists of an enclosure mounted at 4.5 m above ground, including a virtual impactor, parallel plate denuder, and particle supersaturation chamber, connected to the ion chromatography systems via several 20 m perfluoroalkyl sampling lines carrying the dissolved analytes (Markovic et al., 2014). This design reduces artifacts by minimizing the inlet surface area prior to scrubbing the NH_3 from the gas phase in the denuder, and by separating the gas and particle phase constituents while the sample flow is still at ambient temperature and relative humidity (Markovic et al., 2012). In addition, size-resolved, sub-micron non-refractory $NH_{4(p)}$ measurements were taken at 5 minute intervals using an Aerodyne Aerosol Mass Spectrometer (AMS, Liu et al., 2012). We averaged these data to 1 h time resolution in order to compare to the hourly CMAQ model output, which allowed for the evaluation of the ability of CMAQ to simulate the diurnal cycle of NH_3 concentrations. When $NH_{4(p)}$ measurements are available, we compare model results to NH_x to reduce our sensitivity to gas-to-particle partitioning errors in the model; otherwise we compare to $NH_{3(g)}$.

2.3 TES NH_3 retrievals

During CalNex, TES made special observations (transects) near the Bakersfield, CA surface site with a horizontal separation of 12 km on six different afternoons. TES is a nadir-viewing Fourier-transform infrared (FTIR) spectrometer with a high spectral resolution of 0.06 cm^{-1} and a nadir footprint of 5.3 km x 8.3 km. TES flies aboard the NASA Aura spacecraft, which is in a sun-synchronous orbit with an equator crossing time around 01:30 and 13:30 local solar time. Beer et al. (2008) reported the first satellite observations of boundary layer $NH_{3(g)}$ using the TES instrument. Shephard et al. (2011) developed and tested a full $NH_{3(g)}$ retrieval algorithm. The retrieval is based on an optimal estimation approach that minimizes the differences between the TES Level 1B spectra and a radiative transfer calculation that uses absorption coefficients calculated with the AER line-by-line radiative transfer model LBLRTM (Clough et al., 2006). The a priori profiles and covariance matrices for TES NH_3 retrievals are derived from GEOS-Chem model simulations of the 2005 global distribution of NH_3.

The TES $NH_{3(g)}$ retrievals generally have a region of maximum sensitivity between 700 hPa and the surface. While the retrieval is performed on 14 pressure levels, the number of degrees of freedom for signal (DOFS) is generally not greater than one. Therefore at any given single profile level the retrieved volume-mixing ratio (VMR) of NH_3 is highly influenced

by the a priori profile. Rather than attempting to analyse data from individual retrieval levels, it is often desirable to express the retrieved information in a representation where the influence of the a priori is reduced and the information available is collapsed to a single point. To address this issue, Shephard et al. (2011) developed a Representative Volume Mixing Ratio (RVMR) metric for $NH_{3(g)}$ based on similar techniques used previously for CH_4 (e.g., Payne et al., 2009; Wecht et al., 2012; Alvarado et al., 2015) and CH_3OH (e.g., Beer et al., 2008). This RVMR represents a TES sensitivity weighted average value where the influence of the a priori profile is reduced as much as possible; it generally ranges from 20 % to 60 % of the retrieved surface value for $NH_{3(g)}$. The minimum detection level for TES $NH_{3(g)}$ retrievals is an RVMR of approximately 0.4 ppbv, corresponding to a profile with a surface-mixing ratio of about 1-2 ppbv (Shephard et al., 2011).

Pinder et al. (2011) showed that the TES NH_3 retrievals were able to capture the spatial and seasonal variability of NH_3 over eastern North Carolina and that the retrievals compared well with in situ surface observations of NH_3, while Alvarado et al. (2011) showed that TES NH_3 retrievals can also capture the higher concentrations of NH_3 in forest fires in Canada. Sun et al. (2015) demonstrated that under optimal conditions (i.e., good thermal contrast and NH_3 amounts significantly above the TES level of detectability), TES NH_3 agreed very well with in situ aircraft and surface measurements taken in the California Central Valley during the DISCOVER-AQ 2013 campaign.

There are at least three issues that have to be considered when using NH_3 satellite profiles to evaluate model predictions: (a) the vertical resolution of the satellite profile is substantially coarser than that of the model profile; (b) the DOFS for NH_3 are generally less than 1.0; and (c) the retrieved satellite profile reflects the influence of the choice of a priori profile (Rodgers and Connor, 2003). Thus, in order to use these TES observations to evaluate CMAQ model predictions of the concentrations of $NH_{3(g)}$, we first interpolate the hourly CMAQ NH_3 profile predicted for 13:00 local solar time (expressed as the natural logarithm of the mixing ratio) to the TES pressure grid. We then apply the TES observation operator to the interpolated CMAQ NH_3 profile to derive a model TES profile ($\boldsymbol{x}_{\mathrm{TES}}$). Finally, we apply the sensitivity weighting to calculate the model RVMR ($CMAQ_{RVMR}$). This value represents the RVMR that would have been retrieved if (a) TES had sampled a profile identical to the CMAQ-simulated profile and (b) the retrieval errors due to jointly retrieved parameters, other model parameters, and instrument noise were negligible. The observation operator equation is

$$\boldsymbol{x_{TES}} = x_a + \mathbf{A}(\boldsymbol{x_{CMAQ}} - \boldsymbol{x_a}) \quad (1)$$

$$CMAQ_{RVMR} = \mathbf{W} * \boldsymbol{x_{TES}} \quad (2)$$

where $\boldsymbol{x_a}$ is a vector of the TES a priori NH_3 concentrations, $\mathbf{A}$ is the averaging kernel matrix, $\boldsymbol{x_{CMAQ}}$ is a vector of the interpolated CMAQ NH_3 values, and $\mathbf{W}$ is a weighting matrix (Rodgers and Connor, 2003; Payne et al., 2009).

2.4 PBL heights

Several studies have used lidar observations of aerosol profiles to determine the height of the planetary boundary layer (PBL) by identifying regions of large gradients in aerosol concentrations with height (e.g., Tucker et al., 2009; Lewis et al., 2013; Scarino et al., 2014; Hegarty et al., 2015). Scarino et al. (2014) and Tucker et al. (2009) define the mixed layer

measured by the HSRL as 'the volume of atmosphere in which aerosol chemical species emitted within the boundary layer are mixed and dispersed'. The NASA Langley Research Center (LaRC) airborne HSRL measured mixed layer heights during the CalNex campaign and the Carbonaceous Aerosol and Radiative Effects Study (Scarino et al., 2014), both of which we used in this study.

3 Models

3.1 WRF-ARW

CMAQ v5.0.2 was driven with meteorology provided by WRF ARW Version 3.5 (Skamarock and Klemp, 2008) that was configured with 3 nested domains of 36, 12, and 4 km horizontal grid spacing and 41 vertical layers. Shortwave and longwave radiation were calculated using the RRTMG radiative transfer code (Mlawer et al., 1997; Iacono et al., 2008). The YonSie University (YSU, Hong et al., 2006) non-local turbulent PBL scheme and the Noah land surface scheme (Chen and Dudhia, 2001) were used. Initial and boundary conditions for WRF were provided by the North American Regional Reanalysis (NARR, Mesinger et al*.,* 2006), which is recognized as state-of-the-science for North America (Bukovsky and Karoly, 2007). The WRF runs were 32-hour simulations initialized every 24 hours at 0000 UTC with analysis nudging of winds, temperature and humidity above the PBL on the inner 12 km domain as well as winds in the PBL as in Nehrkorn et al. (2013). The WRF outputs for UTC hours 09:00 to 32:00 from each consecutive simulation were combined to form a continuous time series and the initial 8 hours of each simulation were discarded as spin-up time. The 8-h spin-up time and 32-h simulation length is longer than the 6-h spin-up time and 30-h simulation length used by Nehrkorn et al. (2013), but were necessary to perform 24-hour daily CMAQ runs using the 24-h daily CARB emissions files that started at 8:00 UTC. The WRF output was then converted to CMAQ-model-ready files using the Meteorology-Chemistry Interface Processor version 4.2 (MCIP).

3.2 CMAQ

We ran CMAQ on the inner 4 km WRF domain using the SAPRC07 chemical mechanism (Hutzell et al., 2012, Carter et al., 2010ab), which corresponds to the model-ready emission files for CalNex provided by CARB, and with the CMAQ AERO6 aerosol module with aqueous chemistry. Biogenic emissions, photolysis rates, and deposition velocities were all calculated inline. There were few clouds in California during this study period and thus lightning NO_X emissions were negligible; however, lightning NO_x emissions were also calculated inline in CMAQ. Initial and horizontal boundary conditions for CMAQ were provided by GEOS-Chem simulations on a 2° x 2.5° latitude-longitude grid for May and June 2010 following the approach of Lapina et al. (2014).

CMAQ emissions inputs for the state of California were provided as model-ready files by CARB, which prepared them using the Modeling Emissions Data System on a 4 km x 4 km grid-scale (available at http://orthus.arb.ca.gov/calnex/data/calnex2010.html, last accessed June, 2016). The emission change log is provided at

ftp://orthus.arb.ca.gov/pub/outgoing/CalNex/2010/modelready/Change Log for Posted Inventories.pdf (last accessed June, 2016). In this inventory, the NH_3 emissions in SJV are assumed to be constant throughout the day (i.e., no diurnal cycle), and are constant day-to-day in a given month. As the CARB model-ready files had no out-of-state emission sources, our initial simulations were run using the CARB emissions for California, the GEOS-Chem boundary conditions, and no out-of-state emissions. We quantified the potential error in gas-phase $NH_{3(g)}$, Aitken and Accumulation mode aerosol $NH_{4(p)}$, and NH_x in the SJV from neglecting out-of-state agricultural NH_3 emissions by using the agricultural NH_3 emissions from the NEI2011 platform, which we re-gridded from 12 km to our model's 4 km scale while keeping California state emissions constant. We performed this sensitivity test for a 7-day case study between 25-31 May with a 4-day spin up. Adding these out-of-state emissions had a negligible impact on the modelled NH_3 concentrations in the SJV (less than 0.001 % change), as the prevailing winds are mostly out of the north and northwest. Additionally, we tested the effect that errors in the boundary conditions from GEOS-Chem might have on the model runs. Doubling NH_3 boundary conditions for the same 7-day case study also had little impact on NH_3 concentrations in the SJV (less than 0.001 % change), which was expected based on the short lifetime of NH_3.

Finally, we also ran CMAQv5.0.2 using the bi-directional NH_3 flux scheme as developed by Bash et al. (2013) that uses fertilizer application data, crop type, soil type, and meteorology from MCIP output to calculate soil emissions potential and NH_4 to simultaneously calculate NH_3 deposition and emission fluxes for the CMAQ US domain. This scheme uses the U. S. Department of Agriculture's Environmental Policy and Integrated Climate (EPIC) model (Cooter et al., 2012) as contained in the Fertilizer Emissions Scenario Tool (FEST-C).

3.3 HYSPLIT

In order to explore the sources influencing the Bakersfield concentrations we ran the HYSPLIT model. Using meteorological inputs from the WRF 4 km domain discussed in Section 3.1, we generated 36-hour back trajectories with Version 4 of the HYSPLIT model (Draxler and Hess, 1998) initiated from 100 m above ground level (agl) at Bakersfield at 17:00 PDT on June 18th back to 20:00 PDT on June 17th. Results from these runs are briefly discussed in Section 4.1.

4 Model Evaluation

In order to evaluate CMAQ v5.0.2 modelled NH_3 in the SJV we ran three different scenarios for a month long case-study that covers the record of the Bakersfield surface observations (May 22 – June 22, 2010). The model scenarios include: 1) a baseline model run ($CMAQ_{base}$), in which the model was set up as described in Section 3.2, utilizing the CARB emissions inventory; 2) $CMAQ_B$, which ran with the baseline set up but also included the bi-directional NH_3 scheme described in Section 3.2, and finally 3) $CMAQ_{AB}$, which included both the bi-directional NH_3 scheme and diurnally-varying emissions in the SJV, as described in Section 4.1. The following subsections describe the evaluations of all three model scenarios using the three different measurement datasets (surface, aircraft, and satellite) from the CalNex campaign.

4.1 Evaluation of modelled diurnal variability of $NH_{3(g)}$ using surface observations

Table 1 shows that the $CMAQ_{base}$ scenario has a NH_x positive mean bias of 8.24 ppbv over the month-long surface data record; we focus on NH_x so as to minimize the effects of possible model errors in gas-to-particle partitioning on our analysis, as discussed later in this section. However, this bias is not constant throughout the day, as can be seen in the $CMAQ_{base}$ results (blue line) shown in Figure 2. Figure 3a shows the average hourly ratio of $CMAQ_{base}$ modelled NH_x versus measured concentrations for the Bakersfield ground site, averaged over all days of the CalNex campaign; these ratios are derived from the boxplots shown in Figure 3b. The model bias shows a clear diurnal cycle, with $CMAQ_{base}$ significantly overestimating surface NH_x concentrations at night by up to a factor of 4.5 and generally underestimating NH_x during the daytime at 0.6 between 13:00 and 14:00 local time, consistent with the average TES_{RVMR} observations near Bakersfield at about 13:30 local solar time plotted as the green dot in Figure 3a and further discussed in Section 4.3. These results suggest that the constant daily emissions for agricultural NH_3 emissions in the CARB inventory (blue line Figure S1 in the Supplemental Material) may be misrepresenting the diurnal emission patterns suggested by the measurements. This is consistent with previous work done in North Carolina; Wu et al. (2008) found that NH_3 emissions from livestock feed lots show a strong diurnal cycle, peaking at mid-day.

Besides errors in emissions another contributing factor to the modelled bias of $NH_{3(g)}$ could be errors in the gas-to-particle partitioning of $NH_{3(g)}$ to $NH_{4(p)}$. Figure 2a also shows an average hourly plot of the ratio of $CMAQ_{base}$ modelled to measured NH_x and $NH_{3(g)}$ during the campaign. There is very little difference between the two lines, indicating only a small fraction of total $NH_{3(g)}$ is converted into $NH_{4(p)}$ in this region, consistent with Baker et al. (2013). Thus, errors in gas-particle partitioning of NH_3 in CMAQ, while important for accurately estimating $PM_{2.5}$ concentrations, cannot account for the diurnal errors in NH_x we have observed.

Another potential source of diurnal errors in modelled NH_x are diurnal variations in meteorology, which could potentially alter the source regions to which the Bakersfield site was sensitive throughout the day. Differences in NH_3 emission errors at upwind sites would thus appear as diurnal errors in NH_x. We ran a HYSPLIT case study for June 18th, where back trajectories were run for eight different times during the day (Figure S2). As on most days during the CalNex campaign, there is a general flow from the north/north-west that is funnelled through the California Central Valley towards Bakersfield. In these simulations there is no significant change in meteorology with time of day, thus diurnal changes in transport are not likely a contributing factor to the diurnal mismatch shown in modelling results. Thus, these back trajectories, driven with our WRF model, did not show a change in source attribution locations.

Diurnal errors in the PBL height estimates could also potentially be responsible for the diurnal pattern in the CMAQ NH_x concentrations at Bakersfield (Figure 3). We used daytime HSRL measurements taken in the SJV during CalNex to evaluate our WRF simulated PBL heights. Figure 4 shows 2-minute averages of the HSRL calculated mixed layer height compared to the WRF PBL for three daytime flights that passed over the SJV. The modelled and measured heights show good agreement, having a slope of 0.76, r^2 of 0.70, and mean bias of 87 m. Thus errors in daytime PBL height do not seem to account for

much of the underestimate in modelled daytime NH_x. Scarino et al. (2014), when comparing all CalNex HSRL flight measurements to their configuration of the WRF-Chem model, found similar results. In summary, gas-to-particle partitioning and PBL height errors are likely not responsible for the diurnally varying measurement to model biases.

CARB NH_3 emissions in the SJV are constant both diurnally and day-to-day, with an hourly flux of around 0.23 moles s^{-1} for the Bakersfield area (Figure S1). The Bakersfield ground measurements, however, indicate there should be a diurnal pattern of lower emissions at night and higher emissions during the day, as has been previously reported of NH_3 emissions from livestock (e.g., Bash et al., 2013; Zhu et al., 2015a) and other agricultural NH_3 sectors (Skjøth et al., 2011). We tested two methods to improve the diurnal cycle of NH_3 emissions in the CMAQ model. We found that including the bi-directional flux of NH_3 in the $CMAQ_B$ case (green lines) significantly reduces the night-time concentration peaks of NH_3. However there is still a clear model overestimate (mean bias of 4.57 ppb, see Table 1), with the $CMAQ_B$ scenario also causing overestimates following the day's maximum in temperature (Figure 2).

To further improve the model simulations, we applied a scaling factor to all NH_3 area sources per grid box in the SJV, based on the $CMAQ_{base}$ bias relative to the ground measurements. To do this, we first calculated the total NH_3 area source emissions for each grid box, based on additional information on the emissions breakdown from the CARB inventory. For Kern County, where Bakersfield, CA resides, pesticide/fertilizer applications dominate the NH_3 emissions inventory at 72%, followed by farming operations at 25%, and other sources for the remaining fraction. Table S2 in the Supplemental Material describes the fraction of NH_3 emissions for counties in the SJV. We then calculated the emissions for each hour based on the hourly average ground measurements. Note that the adjusted maximum emissions vary by about a factor of 4.5 from the minimum at night to the mid-day peak, as can be seen in Figure S1 (solid red line) which is more modest than the factor of 10 variation seen in livestock feedlots (Bash et al., 2013; J. Bash, personal communication, Oct. 6, 2015). We then reran CMAQ with both these adjusted emissions and the bidirectional NH_3 scheme (the $CMAQ_{AB}$ run) to assess the impact. Despite applying the scaling factor to all emissions instead of solely to the feedlots as in Bash et al. (2013), the $CMAQ_{AB}$ model predictions, shown as the purple lines in Figure 2, matches the measurements (black line) better than the $CARB_{base}$ or $CARB_B$ scenarios over the day and night, consistent with Bash et al. (2013), with the mean night-time bias reduced by about a factor of 2 and the overall bias reduced to -1.23 ppbv (Table 1) and does particularly well between the hours of 01:00 and 06:00. The fact that adding the diurnally-varying emission profile improves the model performance, even though the emissions are dominated by fertilizer applications that should be accounted for by the bi-directional NH_3 scheme, suggests that the scheme in CMAQ v5.0.2 is not correctly accounting for the diurnal variations in NH_3 flux in the SJV.

As noted above, the results for $NH_{3(g)}$ generally track the results for NH_x already discussed. In contrast, the model usually under-predicts the small amount of $NH_{4(p)}$ observed (on average < 1 ppbv, Figure 2c) by a factor of 2, with little variation between the model scenarios (Table 1). These model errors in $NH_{4(p)}$ reflect not only model errors in total NH_x, but also errors in the formation of $HNO_{3(g)}$ and $SO_{4(p)}$ (Figure S3). $HNO_{3(g)}$ is overestimated in all model simulations up to a factor of 4, with concentrations not changing between model cases. $SO_{4(p)}$ measured concentrations are minimal and don't appear to

have any trend and also do not change with model cases. However, as our interest in this study is in constraining NH_3 emissions, not inorganic aerosol formation, we do not investigate these errors further here.

4.2 Evaluation of modelled vertical distribution of $NH_{3(g)}$ using aircraft observations

The aircraft observations in the SJV indicate a large underestimate (range of factors about 1 to 5) in $CMAQ_{base}$ modelled NH_x concentrations at higher altitudes as shown in Table 2 (all flights in SJV) and Figure 5 (two flights). The variation in model concentrations in the background of Figure 5 are due to the aircraft flying in and out of different horizontal grid boxes in the model. The May 24th flight shows a strong $CMAQ_{base}$ NH_x underestimate of about a factor of 5 when considering the entire flight with an r^2 value of 0.31 and mean bias of -1.95 ppbv. This significant underestimate could potentially be due to an underestimate of vertical mixing at night (discussed below); when only data before 18:00 PDT is considered (assuming this is before the collapse of the convective boundary layer) the underestimate is only a factor of ~1.5 and the r^2 is 0.77, a considerably better result. However, model comparisons to flight data on 16 and 18 of June before 18:00 PDT, likely before the boundary layer collapse on these days, also show a significant model underestimate and low r^2 values; thus there may be other contributing factors to this bias. As for the surface observations, the aircraft results for NH_x and $NH_{3(g)}$ are very similar. $NH_{4(p)}$ has a large absolute mean bias for all flights, but its low magnitude has a negligible effect on NH_x concentrations (see Table 2).

Early afternoon (Figure 5a) and evening (Figure 5b) $CMAQ_{base}$ comparisons show a clear difference in the vertical distribution of NH_x. At night (May 24th flight), the model contains most of the NH_x in the lowest model level, whereas during the day (June 16th flight) it vertically mixes the NH_x. These results could suggest 1) vertical mixing is stronger than simulated in the model during both flights, based on the higher NH_x concentrations that the aircraft is measuring at higher altitudes, or 2) that there is a residual layer of NH_x at night that is not captured by the model or 3) there is a non-local source that is also not well captured by the model.

Gas-phase NH_3 can either be deposited to or emitted from the surface depending on the land-type, land-use, and ambient concentrations (Bash et al., 2015; Fowler et al., 2009). The $CMAQ_{base}$ run does not take this into consideration, but when bi-NH_3 is calculated in $CMAQ_{AB}$ and $CMAQ_B$, NH_3 dry deposition should generally decrease, increasing the net land-atmosphere flux (Bash et al., 2013). Figure 5c is consistent with these results (and inconsistent with the hypothesis that vertical mixing is underestimated in the model) as the vertically distributed concentration of NH_x significantly increases from the $CMAQ_{base}$ case to the $CMAQ_B$ case. The transport of NH_3 also tends to increase, this being a potential explanation for the plume entering the plot domain around 21:00 PDT in the bottom curtain plot. The total column concentration of NH_x also increases, leading to a significant positive model bias for the $CMAQ_{AB}$ and $CMAQ_B$ scenarios (e.g. in the earlier part of the flight in Figure 5c and Table 2), suggesting a possible overestimation of total NH_x emissions by the bi-directional NH_3 scheme during the afternoon and evening hours that the flights took place.

4.3 Evaluation of modelled $NH_{3(g)}$ with TES NH_3 retrievals

Figure 6a shows the RVMR retrieved from the TES spectra (TES_{RVMR}) for one overpass (during one hour of model output) on 12 May 2010; the other overpasses during the campaign are similar. Figure 6b shows the equivalent $CMAQ_{base}$ modelled NH_3 RVMR ($CMAQ_{RVMR}$) (see Equation 1 and 2 in Section 2.2), and Figure 6c shows the difference between the two. This figure demonstrates that the $CMAQ_{base}$ case can identify the locations of different sources of NH_3 and the resulting geographical relative changes in NH_3 along the transect, but that the NH_3 RVMRs are underestimated, particularly at higher NH_3 RVMRs (Table 3 and Table S2). Figure 7 shows the modelled and measured RVMR for four transects near Bakersfield between May 22 and June 22 (i.e., during the surface measurement record). The RVMRs for these overpasses are reasonably well correlated (r^2 of 0.64 and mean bias of -2.57 ppbv, Table 3), again suggesting that the $CMAQ_{base}$ inventory does a good job of capturing the spatial distribution of NH_3 emissions near Bakersfield. However the slope of the linear regression of $CMAQ_{base}$ RVMR suggests that CMAQ underestimates high NH_3 concentrations by a factor of 2.4. This demonstrates the importance of using highly time-resolved observations of NH_3 to determine the diurnal cycle of NH_3 along with polar-orbiting satellite retrievals of NH_3 to improve the spatial and seasonal distribution of the emissions, as noted in Zhu et al. (2013). In other words, if we had relied solely on the TES observations at 13:30 local solar time to evaluate the $CMAQ_{base}$ runs, we would have incorrectly assumed that the CARB inventory was a factor of 2.4 too low for total NH_3 emissions, whereas the surface data demonstrate that the problem is primarily in the diurnal cycle of the emissions.

The RVMR bias for these four overpasses changes from -2.57 ppbv to 0.84 ppbv from the $CMAQ_{base}$ run to the $CMAQ_B$ run, respectively (Table 3). The linear regression slope of the observation-model RVMR comparison also improves from 0.47 to 0.93, consistent with the results of Zhu et al. (2015a). Adding adjusted emissions (the $CMAQ_{AB}$ case) increases the RVMR bias to 1.31 ppbv, but improves the regression slope to 1.02. The absolute RVMR bias is thus still better than in the $CMAQ_{base}$ run, but is worse than in the $CMAQ_B$ case.

However, the model RVMR can be very sensitive to errors in the modelled vertical distribution of NH_3. We investigated this by comparing each level of the TES retrieved NH_3 profile with the corresponding CMAQ profile level after the observation operator is applied. Figure 8 shows box-and-whisker plots of this comparison for the $CMAQ_{base}$ and $CMAQ_{AB}$ model scenarios. This plot differs from that in Shephard et al. (2015) in that it includes the average of layers below 908 mb, which introduce an RVMR bias due to levels that are below 1000 mb. For $CMAQ_{base}$, there is a substantial negative bias in the lowest level (-5 ppb), but for $CMAQ_{AB}$ this switches to a positive, smaller bias (~1 ppb). Furthermore, the other, higher levels show little bias (~0.08 ppb). Thus comparing the TES and CMAQ profiles level-by-level indicates that the $CMAQ_{AB}$ scenario performs the best in simulating the TES retrievals, consistent with the conclusions based on the surface observations in Section 4.1.

5 Discussion

The results in Section 4 show that the CMAQ model scenario that included both the bi-directional NH_3 scheme and the diurnally adjusted emissions ($CMAQ_{AB}$) gave results that were much closer to the surface measurements (Section 4.1) and satellite (Section 4.3) observations than the $CMAQ_{base}$ runs, with measurement uncertainties explained in Section 2. The $CMAQ_{AB}$ simulations also resulted in a large overestimate of NH_x concentrations higher in the atmosphere as measured by the aircraft (Section 4.2). Here we discuss the remaining errors in the $CMAQ_{AB}$ scenario, suggest possible explanations for these errors, and make suggestions for the direction of future research.

Both the night-time and daytime simulation of surface NH_x is improved in the $CMAQ_{AB}$ scenario. The total bias is significantly reduced from a factor of 4.5 at night and 0.6 during the day in the $CMAQ_{base}$ scenario (Figure 3a). In $CMAQ_{AB}$, the model does a particularly better job as compared to measurements between the hours of 1:00 am and 6:00 am local time (Figure 9a), perhaps related to the lower emissions at this time of day when adjusted emissions are used. The remaining diurnal bias shows a relative model underestimate with a factor of ~0.6 at 10:00 local time and a relative model overestimate peaking at ~1.7 at 19:00 local time (Figure 9a), with average $CMAQ_{AB}$ modelled concentrations slightly higher in the afternoon and peaking around 19:00 (Figure 9b). It is interesting to note that the $CMAQ_{AB}$ bias relative to surface concentrations is small near the TES overpass time (e.g., crossing 0% between 13:00 and 14:00 local time, Figure 9a), which is consistent with the small bias seen in the comparison with the TES observations in Section 4.3. Furthermore, the aircraft results for the $CMAQ_{AB}$ scenario discussed in Section 4.2 also show a large relative overestimate in the afternoon and evening when the flights took place (Table 2), consistent with the afternoon and evening overestimates seen in the surface data.

Thus all three datasets suggest that the remaining errors in modelled NH_x concentrations are due to the diurnal profile of the net land-atmosphere NH_3 flux in the $CMAQ_{AB}$ run peaking too late in the day. One possibility is that the diurnal cycle we applied to the non-fertilizer NH_3 emissions, which was based on the ambient measurements of NH_3, is peaking too late in the day. However, as the peak of our assumed diurnal profile for these emissions (Figure S1) is consistent with the peak in surface temperature (1:00 pm, Figure 2d), we consider this explanation less likely than remaining errors in the bi-directional NH_3 scheme for fertilizer emissions.

These errors in the bi-directional NH_3 scheme could be due to errors in the dynamic emissions response of the bi-directional NH_3 scheme to local temperature and wind speed conditions (Bash et al., 2013). However, Figure 2d shows that the modelled surface temperature and wind speed are not that far off from the values observed at the Bakersfield site. Thus the remaining errors are less likely related to errors in atmospheric meteorological conditions, and are more likely due to errors in the dependence of soil conditions (e.g., soil temperature, pH, and water content) on meteorology and crop management practices as calculated within the bi-directional NH_3 scheme (Cooter et al., 2012). The scheme calculation assumes two soil layers (0.01 m and 0.05 m) that independently exchange NH_x with the canopy, which then exchanges NH_x with the surface layer of the atmosphere (Bash et al., 2013). If the calculation of the response of soil properties in these

layers to surface meteorology and crop management practices is incorrect (e.g., the soil layers do not heat up or cool down quickly enough with the change in surface temperature), that would affect the amount of NH_x available from the soil as well as the rate at which the soil NH_4^+ is converted to NO_3^- through nitrification (Bash et al., 2013). This would result in errors in the flux of NH_x from the soil to the canopy, thus altering the canopy compensation point and the net atmospheric flux.

The aircraft results may also suggest errors in the vertical mixing of NH_x during the afternoon and evening (e.g., the peak of the PBL height and the collapse). While we consider this effect as likely less important to the remaining errors in $CMAQ_{AB}$ than the potential errors in the bi-directional NH_3 scheme already discussed, an overestimate of vertical mixing during the afternoon would overestimate the flux of NH_x from the surface layer of the atmosphere to the upper levels, consistent with the aircraft overestimate. In addition, the soil-canopy-surface atmosphere system would respond to this overestimate of vertical mixing by increasing the net flux of NH_x from the soil to the atmosphere in order to maintain equilibrium, resulting in a total overestimate of the emissions of NH_x during the afternoon and evening.

We thus recommend that future work to improve the simulation of atmospheric NH_x concentrations in the SJV focus on bottom-up and top-down approaches that will better estimate the diurnal changes in the canopy compensation point that determines the net flux from the land to the atmosphere in the bi-directional NH_3 scheme (Bash et al., 2013). This scheme was originally developed using field scale observations taken in North Carolina, USA (Walker et al., 2013), so it is not surprising that this approach may need modification to work in the SJV. We recommend, first, that the CARB NH_3 inventory be updated to better separate NH_3 emissions from fertilizer and livestock. The Bash et al. (2013) scheme assumes that these two sectors will dominate the NH_3 emissions, while the CARB inventory divides fertilizer/pesticide use from "farming operations", and thus it is unclear if these other farming practices are dominated by livestock or not. Second, the data on crop management (e.g., fertilizer amount, timing, form, and distribution) used in EPIC (and thus in the CMAQ bi-directional NH_3 scheme) is based on data for the entire West Coast of the US (e.g., California, Oregon, and Washington), and thus may not be representative of farming practices in the SJV. Better crop management data specific to the SJV, as well as more SJV-specific data on soil moisture and heating rates, may thus help in removing some of the remaining errors in the $CMAQ_{AB}$ scenario. Third, in order to better connect these bottom-up emission estimates to the measured atmospheric concentrations, we recommend that top-down studies focus not just on correcting the net NH_x flux to the atmosphere but also determine the diurnally-varying biases in the canopy compensation point that determines these net fluxes. This may require the development of adjoint methods and models (e.g., Zhu et al., 2015a) that can retrieve time-varying correction factors for the canopy compensation point, rather than just for the net flux itself.

6 Conclusions

We used NH_3 retrievals from the NASA Tropospheric Emission Spectrometer, as well as surface and aircraft observations of $NH_{3(g)}$ and submicron $NH_{4(p)}$ gathered during the CalNex campaign, to evaluate the ability of the CMAQ model run with the CARB emission inventory to simulate ambient $NH_{3(g)}$ and $NH_{4(p)}$ concentrations in California's San Joaquin Valley. We find

that CMAQ simulations of NH_3 driven with the CARB inventory are qualitatively and spatially consistent with TES satellite observations, with a correlation coefficient (r^2) of 0.64. However, the surface observations at Bakersfield indicate a diurnally varying model bias, with $CMAQ_{base}$ overestimating NH_3 at night by at times more than 50 ppbv and underestimating it during the day by up to 10 ppbv. The surface, satellite, and aircraft observations all suggest that the afternoon NH_3 emissions in the CARB inventory used in $CMAQ_{base}$ are underestimated by at least a factor of two, while the night-time overestimate of NH_3 is likely due to a combination of overestimated night-time NH_3 emissions and underestimated night-time deposition. Thus the diurnally-constant NH_3 emissions used by CARB in the SJV likely misrepresent the diurnal emission cycle.

Using the bi-directional NH_3 scheme in CMAQ ($CMAQ_B$) resulted in reduced NH_x concentrations at night and a slight increase during the day, overall reducing the model bias relative to the surface and satellite observations. However, this scenario substantially increased the simulated mixing ratio of NH_x at higher altitudes, leading to an increased bias relative to the aircraft observations. In addition, errors in the simulation of the night-time surface concentrations remained in this scenario.

In order to further improve the model, we used the surface observations at Bakersfield to derive an empirical diurnal cycle of NH_3 emissions in the SJV in which night-time and midday emissions differed by about a factor of 4.5. Adding this diurnal profile to the CMAQ bi-directional NH_3 simulations ($CMAQ_{AB}$) while keeping the daily total NH_3 emissions constant at the CARB values significantly improved the model performance at night relative to the surface observations, on top of the already improved results from the $CMAQ_B$ simulations. Comparisons with the TES RVMR showed a slight increase in the bias for the $CMAQ_{AB}$ scenario relative to $CMAQ_B$, but further examination of the modelled and retrieved vertical profiles suggests that this is primarily due to ~1 ppb differences in the lowest retrieved level with the $CMAQ_{AB}$ scenario showing little bias (0.08 ppbv) relative to the TES NH_3 profile above this surface level. However, even in the $CMAQ_{AB}$ scenario sizable errors (up to 20 ppbv) in the afternoon and evening NH_3 remained, possibly due to the net land-atmosphere NH_3 flux calculated by the bi-directional NH_3 scheme peaking too late in the day due to errors in the calculated response of the soil conditions (e.g., soil temperature, pH, and water content) to meteorology and crop management practices.

We recommend that future work on modelling NH_x emissions in the SJV include (a) updating the CARB NH_3 inventory to account for NH_3 from fertilizer, livestock, and other farming practices separately, (b) adding information on crop management practices specific to the SJV region to the EPIC-FESTC system, and (c) top-down studies that focus not just on correcting the net NH_x flux to the atmosphere but also on determining the diurnally-varying biases in the canopy compensation point that determines these net fluxes.

Acknowledgements

The authors thank Leo Ramirez and Jeremy Avise at CARB for the emissions inventory data they provided, as well as Eli Mlawer, Thomas Nehrkorn and Elizabeth Steinhubel of AER and Jesse Bash, Jim Kelly, and Kirk Baker of the EPA for their valuable comments and discussions on this work. This work was funded by the NOAA Climate Program Office Atmospheric Chemistry, Carbon Cycle, & Climate (AC4) program through Grants NA130AR4310060 and NA140AR4310129 to CRL, JDH, KCP, and MJA of AER and DKH, MDT, and SLC of CU Boulder. Development and evaluation of the TES NH_3 retrieval was funded through NASA grants to KCP of AER such as Grant NNH08CD52C. LMR acknowledges support from California Air Resources Board (CARB) for funding the AMS measurements (contract 09–328). Infrastructure support for the Bakersfield ground site was provided through CARB contract 08-316 to Ron C Cohen and Allen H Goldstein at the University of California, Berkeley. The collection and analysis of CalNex surface observations of $NH_{3(g)}$ at Bakersfield were funded by a University of Toronto Centre for Global Change Science award to MM and a NSERC graduate scholarship to TCV of the University of Toronto. We also wish to thank the NOAA P3 aircraft flight crew and technicians. The conclusions of this paper are the authors' only, and do not reflect NOAA or CARB policy.

References

Alvarado, M. J., Cady-Pereira, K. E., Xiao, Y., Millet, D. B., and Payne, V. H.: Emission Ratios for Ammonia and Formic Acid and Observations of Peroxy Acetyl Nitrate (PAN) in Biomass Burning Smoke As Seen By the Tropospheric Emission Spectrometer (TES), Atmosphere, 2, 633–654, doi:10.3390/atmos2040633, 2011.

Alvarado, M. J., Payne, V. H., Cady-Pereira, K. E., Hegarty, J. D., Kulawik, S. S., Wecht, K. J., Worden, J. R., Pittman, J. V., and Wofsy, S. C.: Impacts of updated spectroscopy on thermal infrared retrievals of methane evaluated with HIPPO data, Atmos. Meas. Tech., 8, 965–985, doi:10.5194/amt-8-965-2015, 2015.

Bahreini, R., Ervens, B., Middlebrook, A. M., Warneke, C., de Gouw, J. A., DeCarlo, P. F., Jimenez, J. L., Brock, C. A., Neuman, J. A., Ryerson, T. B., Stark, H., Atlas, E., Brioude, J., Fried, A., Holloway, J. S., Peischl, J., Richter, D., Walega, J., Weibring, P., Wollney, A. G., and Fehsenfeld, F. C.: Organic aerosol formation in urban and industrial plumes near Houston and Dallas, Texas, J. Geophys. Res., 114, D00F16, doi:10.1029/2008JD011493, 2009.

Baker, K. R., Misenis, C., Obland, M. D., Ferrare, R. A., Scarino, A. J., and Kelly, J. T.: Evaluation of surface and upper air fine scale WRF meteorological modeling of the May and June 2010 CalNex period in California, Atmos. Environ., doi:10.1016/j.atmosenv.2013.08.006, 2013.

Bash, J. O., Cooter, E. J., Dennis, R. L., Walker, J. T., and Pleim, J. E.: Evaluation of a regional air-quality model with bidirectional NH_3 exchange coupled to an agroecosystem model, Biogeosciences, 10, 1635–1645, doi:10.5194/bg-10-1635-2013, 2013.

Bash, J., Henze, D. K., Jeong, G.-R., Zhu, L., Cady-Pereira, K. E., Shephard, M. W., Luo, M., and Pinder, R. W.: The impact of the diurnal temporal allocation of ammonia emissions on air-quality model estimates of ambient ammonia and inorganic aerosol concentrations, in preparation, 2015. 4827, 4830, 4831

Beer, R., Shephard, M. W., Kulawik, S. S., Clough, S. A., Eldering, A., Bowman, K. W., Sander, S. P., Fisher, B. M., Payne, V. H., Luo, M., Osterman, G. B., and Worden, J. R.: First satellite observations of lower tropospheric ammonia and methanol, Geophys. Res. Lett., 35, L09801, doi:10.1029/2008GL033642, 2008.

Beusen, A. H. W., Bouwman, A. F., Heuberger, P. S. C., Van Drecht, G., and Van der Hoek, K. W.: Bottom-up uncertainty estimates of global ammonia emissions from global agricultural production systems, Atmos. Environ., 42, 6067–6077, 2008.

Bricker, S., Longstaff, B., Dennison, W., Jones, A., Boicourt, K., Wicks, C., and Woerner. J.: Effects of Nutrient Enrichment In the Nation's Estuaries: A Decade of Change. NOAA Coastal Ocean Program Decision Analysis Series No. 26. National Centers for Coastal Ocean Science, Silver Spring, MD, 328 pp, 2007.

Bukovsky, M. S. and Karoly, D. J.: A brief evaluation of precipitation from the North American Regional Reanalysis, J. Hydrometeor., 8, 837–846, 2007.

Carfrae, J. A., Sheppard, L. J., Raven, J., Stein, W., Leith, I. D., Theobald, A., and Crossley, A.: Early effects of atmospheric ammonia deposition on Calluna vulgaris (L.) hull growing on an ombrotrophic peat bog, Water Air Soil Pollut. Focus, 4, 229–239, 2004.

Carmichael, G.R., Tang, Y., Kurata, G., Uno, I., Streets, D., Woo, J.-H., Huang, H., Yienger, J., Lefer, B., Shetter, R., Blake, D., Atlas, E., Fried, A., Apel, E., Eisele, F., Cantrell, C., Avery, M., Barrick, J., Sachse, G., Brune, W., Sandholm, S., Kondo, Y., Singh, H., Talbot, R., Bandy, A., Thorton, D., Clarke, A. and Heikes, B. (2003). Regional-scale chemical transport modeling in support of the analysis of observations obtained during the TRACE-P experiment. Journal of Geophysical Research 108: doi: 10.1029/2002JD003117. issn: 0148-0227.

Carter, W. P. L.: Development of the SAPRC-07 chemical mechanism, Atmos. Environ., 44, 5324–5335, 2010a.

Carter, W. P. L.: Development of a condensed SAPRC-07 chemical mechanism, Atmos. Environ., 44, 5336–5345, 2010b.

Chen, F. and Dudhia, J.: Coupling an advanced land-surface–hydrology model with the Penn State–NCAR MM5 modeling system. Part I: Model implementation and sensitivity, Mon. Wea. Rev., 129, 569–586, 2001.

Clarisse, L., Coheur, P.-F., Prata, F., Hadji-Lazaro, J., Hurtmans, D., and Clerbaux, C.: A unified approach to infrared aerosol remote sensing and type specification, Atmos. Chem. Phys., 13, 2195-2221, doi:10.5194/acp-13-2195-2013, 2013.

Clough, S. A., Shephard, M. W., Worden, J., Brown, P. D., Worden, H. M., Mingzhao, L., Rodgers, C. D., Rinsland, C.P., Goldman, A., Brown, L., Kulawik, S. S., Eldering, A., Lampel, M., Osterman, G., Beer, R., Bowman, K., Cady-Pereira, K. E., and Mlawer, E. J.: Forward Model and Jacobians for Tropospheric Emission Spectrometer Retrievals, IEEE Trans. Geosci. Remote Sens., 44, 1308–1323, 2006.

Cooter, E. J., Bash, J. O., Benson, V., and Ran, L.: Linking agri- cultural crop management and air quality models for regional to national-scale nitrogen assessments, Biogeosciences Discuss., 9, 6095–6127, doi:10.5194/bgd-9-6095-2012, 2012.

Draxler, R. R. and. Hess, G. D.: An overview of the HYSPLIT_4 modeling system for trajectories, dispersion, and deposition, Aust. Meteorol. Mag., 47, 295–308, 1998.

Ellis, R. A., Murphy, J. G, Pattey, E., van Haarlem, R., O'Brien, J. M., and Herndon, S. C.: Characterizing a Quantum Cascade Tunable Infrared Laser Differential Absorption Spectrometer (QC-TILDAS) for measurements of atmospheric ammonia, Atmos. Meas. Tech., 3, 397–406, 2010.

Ellis, R. A., Murphy, J. G., Markovic, M. Z., VandenBoer, T. C., Makar, P. A., Brook, J., and Mihele, C.: The influence of gas-particle partitioning and surface-atmosphere exchange on ammonia during BAQS-Met, Atmos. Chem. Phys., 11, 133–145, doi:10.5194/acp-11-133-2011, 2011.

Fowler, D., Pilegaard, K., Sutton, M., Ambus, P., Raivonen, M., Duyzer, J., Simpson, D., Fagerli, H., Fuzzi, S., Schjoerring, J., Granier, C., Neftel, A., Isaksen, I., Laj, P., Maione, M., Monks, P., Burkhardt, J., Daemmgen, U., Neirynck, J., Personne, E., Wichink-Kruit, R., Butterbach-Bahl, K., Flechard, C., Tuovinen, J., Coyle, M., Gerosa, G., Loubet, B., Altimir, N., Gruenhage, L., Ammann, C., Cieslik, S., Paoletti, E., Mikkelsen, T., Ro-Poulsen, H., Cellier, P., Cape, J., Horvath, L., Loreto, F., Niinemets, U., Palmer, P., Rinne, J., Misztal, P., Nemitz, E., Nilsson, D., Pryor, S., Gallagher, M., Vesala, T., Skiba, U., Brueggemann, N., Zechmeister-Boltenstern, S., Williams, J., O'Dowd, C., Facchini, M., de Leeuw, G., Flossman, A., Chaumerliac, N., and Erisman, J.: Atmospheric composition change: Ecosystems-Atmosphere interactions, Atmos. Environ., 43, 5193–5267, doi:10.1016/j.atmosenv.2009.07.068, 2009.

Galloway, J. N., Townsend, A. R., Erisman, J. W., Bekunda, M., Cai, Z., Freney, J. R., Martinelli, L. A., Seitzinger, S. P., and Sutton, M. A.: Transformation of the Nitrogen Cycle: Recent Trends, Questions, and Potential Solutions, Science, 320, 889– 892, 2008.

Gilliland, A. B., Dennis, R. L., Roselle, S. J., and Pierce, T. E.: Seasonal NH3 emission estimates for the eastern United States based on ammonium wet concentrations and an inverse modeling method, J. Geophys. Res., 108, D15, 4477, doi:10.1029/2002jd003063, 2003.

Gilliland, A. B., Wyat Appel, K., Pinder, R. W., and Dennis, R. L.: Seasonal NH3 emissions for the continental United States: Inverse model estimation and evaluation, Atmos. Environ., 40, 4986–4998, 2006.

Heald, C. L., Collett Jr., J. L., Lee, T., Benedict, K. B., Schwandner, F. M., Li, Y., Clarisse, L., Hurtmans, D. R., Van Damme, M., Clerbaux, C., Coheur, P.-F., Philip, S., Martin, R. V., and Pye, H. O. T.: Atmospheric ammonia and particulate inorganic nitrogen over the United States, Atmos. Chem. Phys., 12, 10295–10312, doi:10.5194/acp-12-10295-2012, 2012.

Hegarty, J., Henderson, J., Lewis, J., McGrath-Spangler, E., Scarino, A. J., Ferrare, R., P. DeCola, P., and Welton, E.: Evaluating High-Resolution WRF Simulations of PBL Depth Using Observations from DISCOVER-AQ 2011, Meteorology and Climate – Modeling for Air Quality, September 16-18, 2015, Sacramento, CA, 2015.

Hensen, A., Loubet, B., Mosquera, J., van den Bulk, W. C. M., Erisman, J. W., Dämmgen, U., Milford, C., Löpmeier, F. J., Cellier, P., Mikuška, P., and Sutton, M.A.: Estimation of NH_3 emissions from a naturally ventilated livestock farm using local-scale atmospheric dispersion modelling, *Biogeosciences,* 6, 2847–2860, 10.5194/bg-6-2847-2009, 2009.

Henze, D. K., Seinfeld, J. H., and Shindell, D. T.: Inverse modeling and mapping US air quality influences of inorganic PM2.5 precursor emissions using the adjoint of GEOS-Chem, Atmos. Chem. Phys., 9, 5877–5903, 2009.

Hong, S.-Y., Noh, Y., and Dudhia, J.: A new vertical diffusion package with an explicit treatment of entrainment processes, Mon. Wea. Rev., 134, 2318–2341, 2006.

Hristov, A. N., Hanigan, M., Cole, A., Todd, R., McAllister, T. A., Ndegwa, P. M., and Rotz, A.: Review: Ammonia emissions from dairy farms and beef feedlots, Can. J. Anim. Sci., 91(1), 1–35, doi:10.4141/CJAS10034, 2011.

Hutzell, W. T., Luecken, D. J., Appel, K. W., and Carter, W. P. L.: Interpreting predictions from the SAPRC07 mechanism based on regional and continental simulations, Atmos. Environ., 46, 417– 429, 2012.

Iacono, M. J., Delamere, J. S., Mlawer, E. J., Shephard, M. W., Clough, S. A., and Collins, W. D: Radiative forcing by long-lived greenhouse gases: Calculations with the AER radiative transfer models, J. Geophys. Res., 113, D13103, 2008.

Kelly, J. T., Baker, K. B., Nowak, J. B., Murphy, J. G., Markovic, M. Z., VandenBoer, T. C., Ellis, R. A., Neuman, J. A., Weber, R. J., Roberts, J. M., Veres, P. R., de Gouw, J. A., Beaver, M. R., Newman, S., and Misenis, C.: Fine-scale simulation of ammonium and nitrate over the South Coast Air Basin and San Joaquin Valley of California during CalNex-2010, J. Geophys. Res. Atmos., 119(6), 3600–3614. ISSN 2169-897X. 2014.

Langford, A. O., Fehsenfeld, F. C., Zachariassen, J., and Schimel, D. S.: Gaseous ammonia fluxes and background concentrations in terrestrial ecosystems of the United States, Global Biogeochem. Cy., 6, 459–483, 1992.

Lapina, K., Henze, D. K., Milford, J. B., Huang, M., Lin, M., Fiore, A. M., Carmichael, G., Pfister, G., and Bowman, K.: Assessment of source contributions to seasonal vegetative exposure to ozone in the U.S., J. Geophys. Res. Atmos., 119, 324–340, doi:10.1002/2013JD020905, 2014.

Lewis, J. R., E. J. Welton, A. M. Molod, and E. Joseph: Improved boundary layer depth retrievals from MPLNET, J. Geophys. Res. Atmos., 118, 9870–9879, doi:10.1002/jgrd.50570, 2013.

Liu, S., L. Ahlm, D.A. Day, L.M. Russell, Y.L. Zhao, D.R. Gentner, R.J. Weber, A.H. Goldstein, M. Jaoui, J.H. Offenberg, T.E. Kleindienst, C. Rubitschun, J.D. Surratt, R.J. Sheesley, and S. Scheller, Secondary Organic Aerosol Formation from Fossil Fuel Sources Contribute Majority of Summertime Organic Mass at Bakersfield, Journal of Geophysical Research – Atmospheres, 117: doi:10.1029/2012jd018170, 2012.

Lonsdale, C. R., Stevens, R. G., Brock, C. A., Makar, P. A., Knipping, E. M., and Pierce, J. R.: The effect of coal-fired power-plant SO_2 and NO_X control technologies on aerosol nucleation in the source plumes, Atmos. Chem. Phys., 12, 2012, doi:10.5194/acp-12-11519-2012.

Markovic, M. Z., VandenBoer, T. C., and Murphy, J. G.: Characterization and optimization of an online system for the simultaneous measurement of atmospheric water-soluble constituents in the gas and particle phases, J. Environ. Monit., 14, 1872–1884, 2012.

Markovic, M. Z., T. C. VandenBoer, K. R. Baker, J. T. Kelly, and J. G. Murphy, Measurements and modeling of the inorganic chemical composition of fine particulate matter and associated precursor gases in California's San Joaquin Valley during CalNex 2010, J. Geophys. Res. Atmos., 119, doi:10.1002/ 2013JD021408.

Martin, S. T., Hung, H.-M., Park, R. J., Jacob, D. J., Spurr, R. J. D., Chance, K. V., and Chin, M.: Effects of the physical state of tropospheric ammonium-sulfate-nitrate particles on global aerosol direct radiative forcing, Atmos. Chem. Phys., 4, 183–214, doi:10.5194/acp-4-183-2004, 2004.

Mesinger, F., DiMego, G., Kalnay, E., Mitchell, K., Shafran, P. C., Ebisuzaki, W., Jovic, D., Woollen, J., Rogers, E., and Berbery, E. H.: North American regional reanalysis, B. Am. Meteorol. Soc., 87, 343–360, 2006.

Mlawer, E. J., Taubman, S. J., Brown, P. D., Iacono, M. J., and Clough, S. A.: RRTM, a validated correlated-k model for the longwave, J. Geophys. Res., 102, 16663–16682, 1997.

Moss, R. H., Edmonds, J. A., Hibbard, K. A., Manning, M. R., Rose, S. K., van Vuuren, D. P., Carter, T. R., Emori, S., Kainuma, M., Kram, T., Meehl, G. A., Mitchell, J. F. B., Nakicenovic, N., Riahi, K., Smith, S. J., Stouffer, R. J., Thomson, A. M., Weyant, J. P., and Wilbanks, T. J.: The next generation of scenarios for climate change research and assessment, Nature, 463, 747–756, doi:10.1038/nature08823, 2010.

Nehrkorn, T., Henderson, J., Leidner, M., M. Mountain, J. Eluszkiewicz, K. McKain, and S. C. Wofsy: WRF simulations of the urban circulation in the Salt Lake City area for CO_2 modeling, J. Appl. Meteor. Clim., 52, 323–340, 2013.

Nemitz, E., Milford, C., and Sutton, M. A.: A two-layer canopy compensation point model for describing bi-directional biosphere-atmosphere exchange of ammonia, Q. J. Roy. Meteor. Soc., 127, 815–833, 2001.

Nowak, J.B. et al., A Chemical Ionization Mass Spectrometry Technique for Airborne Measurements of Ammonia, J. Geophys. Res., 112, D10S02, doi:10.1029/2006JD007589, 2007.

Nowak, J. B., Neuman, J. A., Bahreini, R., Brock, C. A., Middlebrook, A. M., Wollny, A. G., Holloway, J. S., Peischl, J., Ryerson, T. B., and Fehsenfeld, F. C.: Airborne observations of ammonia and ammonium nitrate formation over Houston, Texas, J. Geophys. Res., 115, D22304, doi:10.1029/2010JD01495, 2010.

Nowak, J. B., Neuman, J. A., Bahreini, R., Middlebrook, A. M., Holloway, J. S., McKeen, S. A., Parrish, D. D., Ryerson, T. B., and Trainer, M.: Ammonia sources in the California South Coast Air Basin and their impact on ammonium nitrate formation, Geophys. Res. Lett., 39, L07804, doi:1029/2012GL051197, 2012.

Paulot, F. and Jacob, D. J.: Hidden Cost of U.S. Agricultural Exports: Particulate Matter from Ammonia Emissions, Environ. Sci. Technol., 48(2), 903–8, doi: 10.1021/es4034793, 2014.

Payne, V. H., Clough, S. A., Shephard, M. W., Nassar, R., and Logan, J. A.: Information-centered representation of retrievals with limited degrees of freedom for signal: Application to methane from the Tropospheric Emission Spectrometer, J. Geophys. Res., 114, D10307, doi:10.1029/2008JD010155, 2009.

Pinder, R. W., Walker, J. T., Bash, J. O., Cady-Pereira, K. E., Henze, D. K., Luo, M., Osterman, G. B., and Shephard, M. W.: Quantifying spatial and seasonal variability in atmospheric ammonia with in situ and space-based observations, Geophys. Res. Lett., 38, L04802, doi:10.1029/2010GL046146, 2011.

Pope, C. A., Burnett, R. T., Thurston, G. D., Thun, M. J., Calle, E. E., Krewski, D., and Godleski, J. J.: Cardiovascular Mortality and Year-round Exposure to Particulate Air Pollution: epidemiological evidence of general pathophysiological pathways of disease, Circulation, 109, 71–77, 2004.

RoTAP: Review of Transboundary Air Pollution: Acidification, Eutrophication, Ground Level Ozone and Heave Metals in the UK. Contract Report to the Department for Environment, Food and Rural Affairs. Centre for Ecology & Hydrology, 2012.

Rodgers, C. D. and Connor, B. J.: Intercomparison of remote sounding instruments, J. Geophys. Res., 108, doi:10.1029/2002JD002299, 2003.

Ryerson, T. B., Andrews, A. E., Angevine, W. M., Bates, T. S., Brock, C. A., Cairns, B., Cohen, R. C., Cooper, O. R., de Gouw, J. A., Fehsenfeld, F. C., Ferrare, R. A., Fischer, M. L., Flagan, R. C., Goldstein, A. H., Hair, J. W., Hardesty, R. M., Hostetler, C. A., Jimenez, J. L., Langford, A. O., McCauley, E., McKeen, S. A., Molina, L. T., Nenes, A., Oltmans, S. J., Parrish, D. D., Pederson, J. R., Pierce, R. B., Prather, K., Quinn, P. K., Seinfeld, J. H., Senff, C. J., Sorooshian, A., Stutz, J., Surratt, J. D., Trainer, M., Volkamer, R., Williams, E. J., and Wofsy, S. C: The 2010 California Research at the Nexus of Air Quality and Climate Change (CalNex) field study, J. Geophys. Res. Atmos., 118, 5830–5866, doi:10.1002/jgrd.50331, 2013.

Sawycky, M., Boulton, J. W., Trask, T., Van Heyst, B., and McClellan, C.: BC Agricultural Air Emissions Inventory. Rep. No. 1302423. Vancouver: RWDI, 2014, BC Ministry of Agriculture, 2014.

Scarino, A. J., Obland, M. D., Fast, J. D., Burton, S. P., Ferrare, R. A., Hostetler, C. A., Berg, L. K., Lefer, B. L., Haman, C. L., Rogers, R. R., Butler, C. F., Cook, A. L., and Harper, D. B.: Comparison of mixed layer heights from airborne high spectral resolution lidar, ground-based measurements, and the WRF-Chem model during CalNex and CARES, Atmos. Chem. Phys., 14, 5547–5560, doi:10.5194/acp-14-5547-2014, 2014.

Schiferl, L. D., Heald, C. L., Nowak, J. B., Holloway, J. S., Neuman, J. A., Bahreini, R., Pollack, I. B., Ryerson, T. B., Wiedinmyer, C., and Murphy, J. G.: An investigation of ammonia and inorganic particulate matter in California during the CalNex campaign, J. Geophys. Res. Atmos., 119, 1883–1902, doi:10.1002/2013JD020765, 2014.

Schlesinger, W.H., 2009. On the fate of anthropogenic nitrogen. Proceedings of the National Academy of Sciences, U.S 106, 203e208.

Shephard, M. W., Cady-Pereira, K. E., Luo, M., Henze, D. K., Pinder, R. W., Walker, J. T., Rinsland, C. P., Bash, J. O., Zhu, L., Payne, V. H., and Clarisse, L.: TES ammonia retrieval 25 strategy and global observations of the spatial and seasonal variability of ammonia, Atmos. Chem. Phys., 11, 10743–10763, doi:10.5194/acp-11-10743-2011, 2011.

Shephard, M. W. and Cady-Pereira, K. E.: Cross-track Infrared Sounder (CrIS) satellite measurements of tropospheric ammonia, Atmos. Meas. Tech., 8, 1323–1336, 2015 www.atmos-meas-tech.net/8/1323/2015/ doi:10.5194/amt-8-1323-2015, 2015.

Shephard, M. W., McLinden, C. A., Cady-Pereira, K. E., Luo, M., Moussa, S. G., Leithead, A., Liggio, J., Staebler, R. M., Akingunola, A., Makar, P., Lehr, P., Zhang, J., Henze, D. K., Millet, D. B., Bash, J. O., Zhu, L., Wells, K. C., Capps, S. L., Chaliyakunnel, S., Gordon, M., Hayden, K., Brook, J. R., Wolde, M., and Li, S.-M.: Tropospheric Emission Spectrometer (TES) satellite observations of ammonia, methanol, formic acid, and carbon monoxide over the Canadian oil sands: validation and model evaluation, Atmos. Meas. Tech., 8, 5189-5211, doi:10.5194/amt-8-5189-2015, 2015.

Simon, H., Allen, D. T., and Wittig, A. E.: Fine particulate matter emissions inventories: Comparisons of emissions estimates with observations from recent field programs, J. Air & Waste Manage. Assoc., 58, 320–343, 2008.

Skamarock, W. C. and Klemp, J. B.: A time-split nonhydrostatic atmospheric model for weather research and forecasting applications, J. Comp. Phys., 227, 3465–3485, 2008.

Skjøth, C. A., Geels, C., Berge, H., Gyldenkærne, S., Fagerli, H., Ellermann, T., Frohn, L. M., Christensen, J., Hansen, K. M., Hansen, K., and Hertel, O.: Spatial and temporal variations in ammonia emissions – a freely accessible model code for Europe, Atmos. Chem. Phys., 11, 5221-5236, doi:10.5194/acp-11-5221-2011, 2011.

Skjøth, C. A. and Geels, C.: The effect of climate and climate change on ammonia emissions in Europe, Atmos. Chem. Phys., 13, 117-128, doi:10.5194/acp-13-117-2013, 2013.

Sun, K., Cady-Pereira, K., Miller, D. J., Tao, L., Zondlo, M. A., Nowak, J. B., Neuman, J. A., Mikoviny, T., Müller, M., Wisthaler, A., Scarino, A. J., and Hostetler, C. A.: Validation of TES ammonia observations at the single pixel scale in the San Joaquin Valley during DISCOVER-AQ, J. Geophys. Res. Atmos., 120, 5140–5154. doi: 10.1002/2014JD022846., 2015.

Tucker, S. C., Brewer, Wm. A., Banta, R. M., Senff, C. J., Sandberg, S. P., Law, D. C., Weickmann, A., and Hardesty, R. M. :Doppler lidar estimation of mixing height using turbulence, shear, and aerosol profiles, J. Atmos. Ocean Tech., 26, 673–688, 2009.

Van Damme, M., Clarisse, L., Heald, C. L., Hurtmans, D., Ngadi, Y., Clerbaux, C., Dolman, A. J., Erisman, J. W., and Coheur, P. F.: Global distributions, time series and error characterization of atmospheric ammonia (NH3) from IASI satellite observations, Atmos. Chem. Phys., 14, 2905–2922, doi:10.5194/acp-14-2905-2014, 2014.

Walker, J. M., Seinfeld, J. H., Clarisse, L., Coheur, P.-F., Clerbaux, C., and Van Damme, M.: Simulation of nitrate, sulfate, and ammonium aerosols over the United States, Atmos. Chem. Phys. Discuss., 12, 19499–19527, doi:10.5194/acpd-12-19499- 2012, 2012.

Walker, J. T., Jones, M. R., Bash, J. O., Myles, L., Meyers, T., Schwede, D., Herrick, J., Nemitz, E., and Robarge, W.: Processes of ammonia air–surface exchange in a fertilized *Zea mays* canopy, Biogeosciences, 10, 981–998, doi:10.5194/bg-10-981-2013, 2013.

Wecht, K. J., Jacob, D. J., Wofsy, S. C., Kort, E. A., Worden, J. R., Kulawik, S. S., Henze, D. K., Kopacz, M., and Payne, V. H.: Validation of TES methane with HIPPO aircraft observations: implications for inverse modeling of methane sources, Atmos. Chem. Phys., 12, 1823–1832, doi:10.5194/acp-12-1823-2012, 2012.

Wichink Kruit, R. J., Schaap, M., Sauter, F. J., van Zanten, M. C., and van Pul, W. A. J.: Modeling the distribution of ammonia across Europe including bi-directional surface–atmosphere exchange, Biogeosciences, 9, 5261-5277, doi:10.5194/bg-9-5261-2012, 2012.

World Health Organization, Health Effects of Particulate Matter, Europe, available at: http://www.euro.who.int/__data/assets/pdf_file/0006/189051/, last accessed: January 2016.

Wu, S-Y., Hub, J.-L., Zhang, Y., and Aneja, V. P.: Modeling atmospheric transport and fate of ammonia in North Carolina—Part II: Effect of ammonia emissions on fine particulate matter formation, Atmos. Environ., 42, 3437–3451, 2008.

Zhang, L., Wright, P. L., and Asman, W. A. H.: Bi-directional air-surface exchange of atmospheric ammonia – A review of measurements and a development of a big-leaf model for applications in regional-scale air-quality models, J. Geophys. Res., 115, D20310, doi:10.1029/2009JD013589, 2010.

Zhu, L., Henze, D. K., Cady-Pereira, K. E., Shephard, M. W., Luo, M., Pinder, R. W., Bash, J. O., and Jeong, G. R.: Constraining U.S. ammonia emissions using TES remote sensing observations and the GEOS-Chem adjoint model, J. Geophys. Res. Atmos., 118, 3355–3368, doi:10.1002/jgrd.50166, 2013.

Zhu, L., Henze, D., Bash, J., Jeong, G.-R., Cady-Pereira, K., Shephard, M., Luo, M., Paulot, F., and Capps, S.: Global evaluation of ammonia bi-directional exchange, Atmos. Chem. Phys. Discuss., 15, 4823–4877, doi:10.5194/acpd-15-4823-2015, 2015a.

Zhu, L., D. K. Henze, J. O. Bash, K. E. Cady-Pereira, M. W. Shephard, M. Luo, and S. L. Capps: Sources and impacts of atmospheric NH3: Current understanding and frontiers for modeling, measurements, and remote sensing in North America, Current Pollution Reports, 1(2), 95–116, 2015b.

Table 1. Summary statistics of the modelled NH_x, $NH_{3(g)}$ and $NH_{4(p)}$ concentration comparisons to the ground measurements for all three model runs.

	NHx				$NH_{3(g)}$		$NH_{4(p)}$	
Model Run	Slope	r^2	MB (ppbv)	MNB (%)	MB (ppbv)	MNB (%)	MB (ppbv)	MNB (%)
$CMAQ_{base}$	-2.49+/-0.15	0.001	8.24	72.54	8.63	78.79	-0.40	-52.96
$CMAQ_B$	1.22+/-0.07	0.01	4.57	45.74	4.99	50.60	-0.41	-55.92
$CMAQ_{AB}$	0.85+/-0.05	0.05	-1.23	-10.70	-0.79	-14.01	-0.44	-60.24

Table 2. Summary statistics of the modelled to measured NH_x concentration comparisons following the SJV flights.

		NH_x				**$NH_{3(g)}$**		**$NH_{4(p)}$**	
Date	**Time (PDT)**	**Slope**	**r^2**	**MB (ppbv)**	**MNB (%)**	**MB (ppbv)**	**MNB (%)**	**MB (ppbv)**	**MNB (%)**
$CMAQ_{base}$									
20100524	16:00-22:00	0.20+/-0.01	0.31	-1.95	-2.010	-1.74	-18.24	-0.14	-58.70
	16:00-18:00	0.68+/-0.05	0.77	-0.20	-10.79	-0.04	-32.46	-0.08	-53.19
	18:00-22:00	0.18+/-0.01	0.29	-2.40	-0.213	-2.24	-14.65	-0.14	-60.10
20100616	13:00-18:00	0.30+/-0.02	0.43	-5.92	-8.980	-4.90	-3.59	-0.24	-45.32
20100618	13:00-18:00	0.18+/-0.02	0.10	-8.12	-18.97	-7.85	-28.9	-0.26	-75.20
$CMAQ_B$									
20100524	16:00-22:00	0.36+/-0.03	0.09	5.56	351.82	5.71	453.86	-0.10	-39.32
	16:00-18:00	-1.57+/-0.24	0.19	6.59	506.18	6.71	639.07	-0.07	-31.92
	18:00-22:00	0.31+/-0.03	0.11	5.30	31.28	5.46	407.1	-0.11	-41.18
20100616	13:00-18:00	0.76+/-0.06	0.04	6.27	248.03	6.63	279.85	-0.22	-33.82
20100618	13:00-18:00	0.37+-0.04	0.02	4.26	394.88	4.41	458.88	-0.21	-52.37
$CMAQ_{AB}$									
20100524	16:00-22:00	0.38+/-0.03	0.17	6.15	369.73	6.30	474.89	-0.10	-38.48
	16:00-18:00	-1.61+/-0.25	0.16	6.94	526.88	7.07	664.26	-0.07	-31.17
	18:00-22:00	0.32+/-0.02	0.22	5.95	330.05	6.10	427.07	-0.11	-40.33
20100616	13:00-18:00	0.80+/-0.06	0.10	7.83	264.1	8.19	297.58	-0.22	-33.83
20100618	13:00-18:00	0.42+/-.05	0.03	5.59	425.7	5.76	494.16	-0.21	-50.36

Table 3. Summary statistics of the $CMAQ_{RVMR}$ to TES_{RVMR} NH_3 comparisons for 4 CalNex overpasses (05/28, 05/30, 06/13, 06/15).

Model Run	**Slope**	**r^2**	**MB (ppbv)**	**MNB (%)**
$CMAQ_{base}$	0.47	0.64	-2.57	-30.21
$CMAQ_{B}$	0.93	0.60	0.84	14.40
$CMAQ_{AB}$	1.02	0.60	1.31	19.57

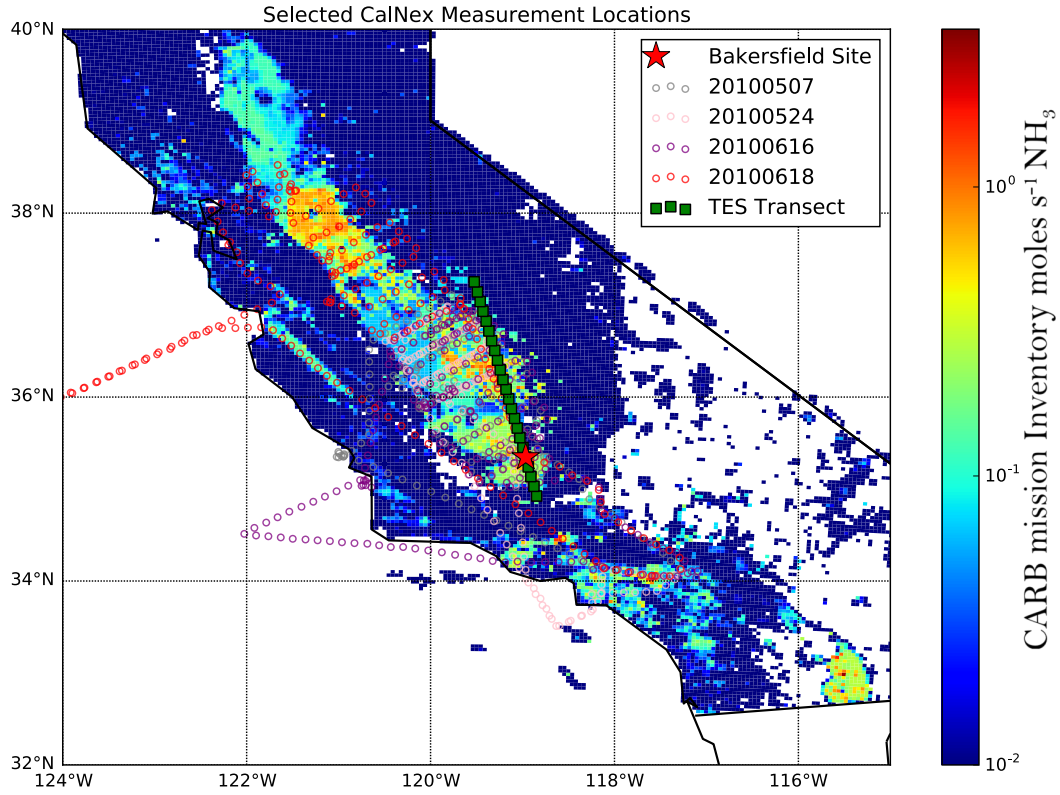

Figure 1. Distribution of NH_3 emissions across California (background) on May 12, 2010 at 19:00 UTC as well as P3 flight tracks (small circles), TES transect (green squares), and the Bakersfield site (red star)

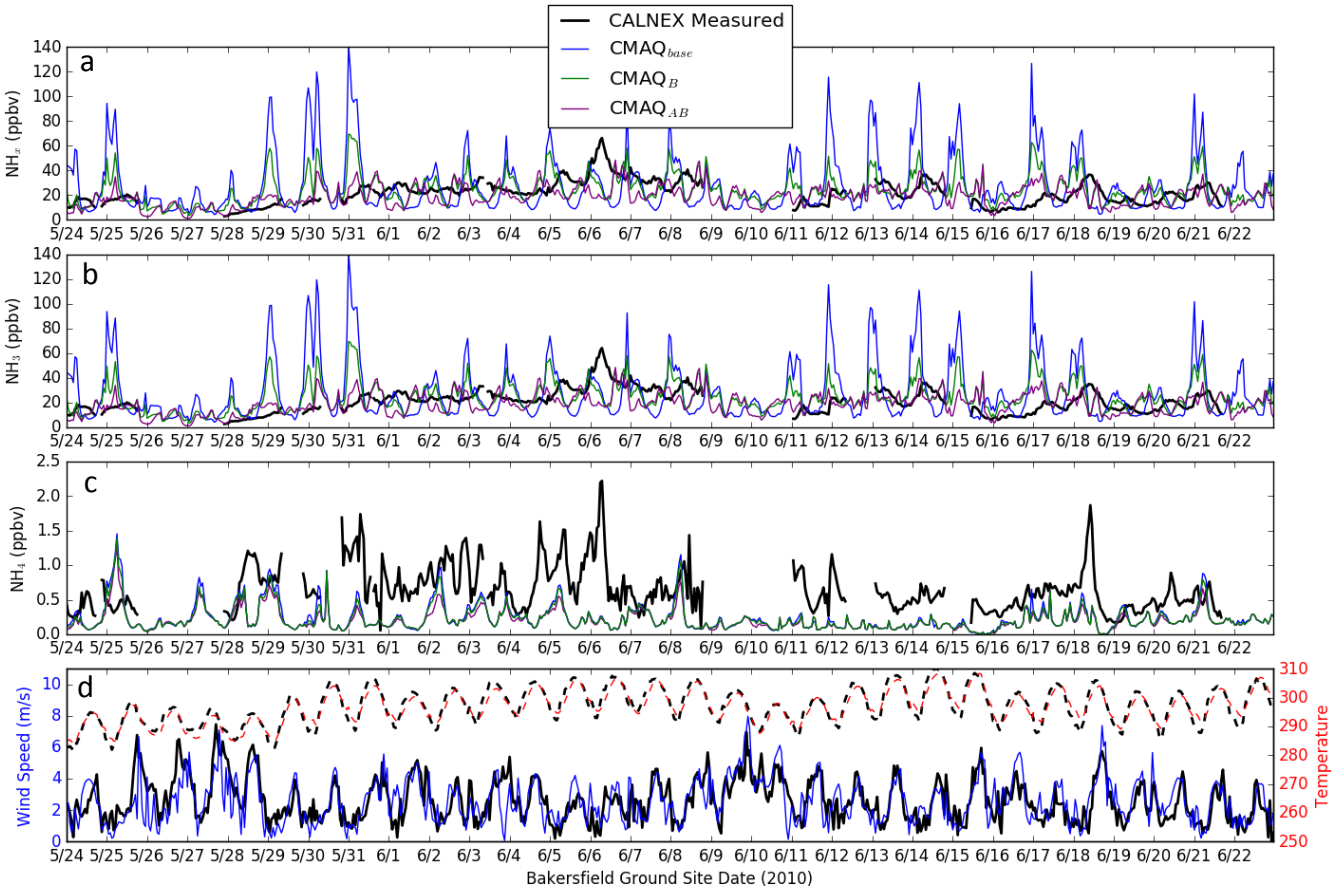

Figure 2. The CalNex ground measurements at the Bakersfield site (solid black) compared to the $CMAQ_{base}$ (solid blue), $CMAQ_{AB}$ (purple) and $CMAQ_{B}$ (green) simulations for a month of model runs. The top panel (a) shows NH_x, b) shows $NH_{3(g)}$, c) $NH_{4(p)}$, and d) wind speed on the left and temperature on the right axis.

5

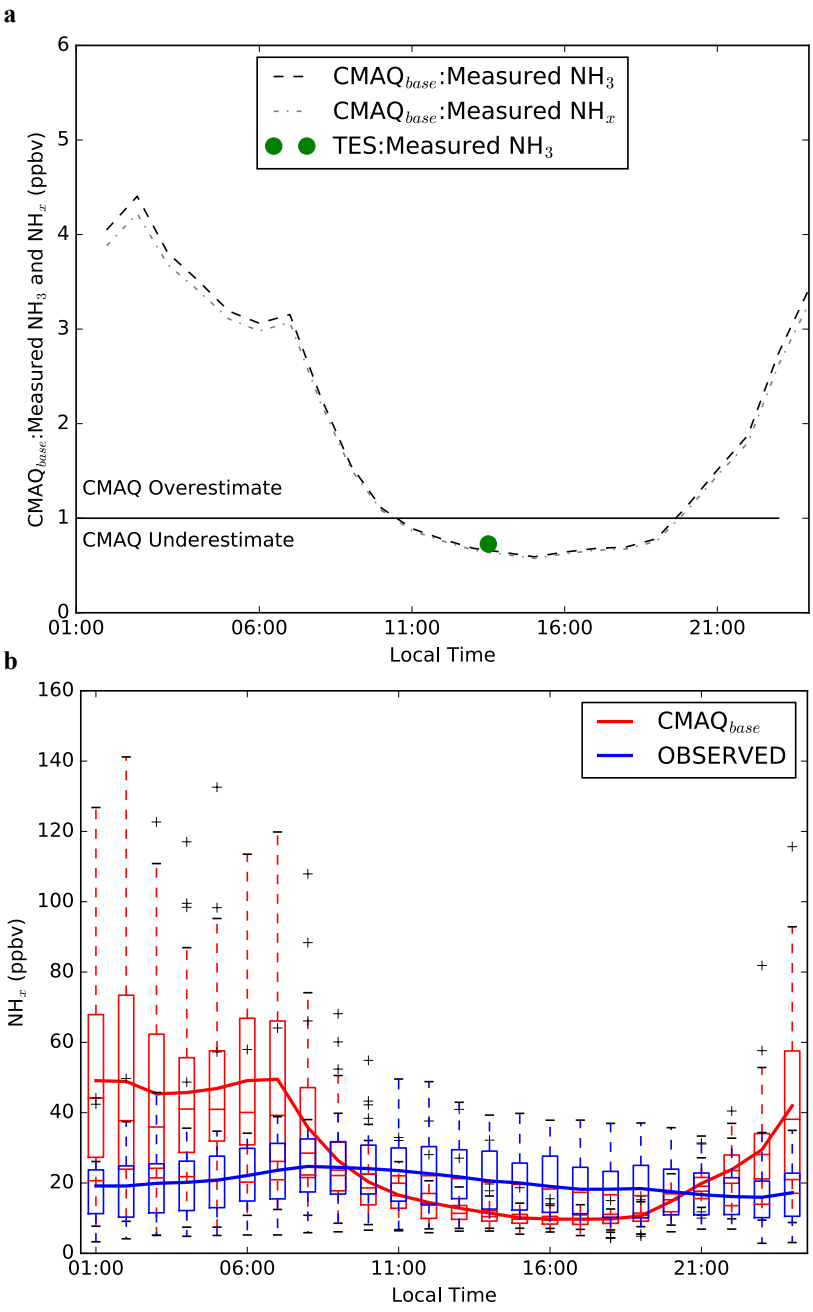

Figure 3. a) The average hourly ratio of modelled to measured NH_3 (dashed-dotted line) and NH_x (dashed line) mixing ratios at the Bakersfield ground site and the average modelled RVMR to TES RVMR ratio (green dot) in local PDT. b) Boxplot of average hourly modelled (red) and measured (blue) NH_x mixing ratios for the Bakersfield ground site, averaged over all measurement days during CalNex where the boxplots show the inter-quartile range and median line within the box and outliers (whiskers).

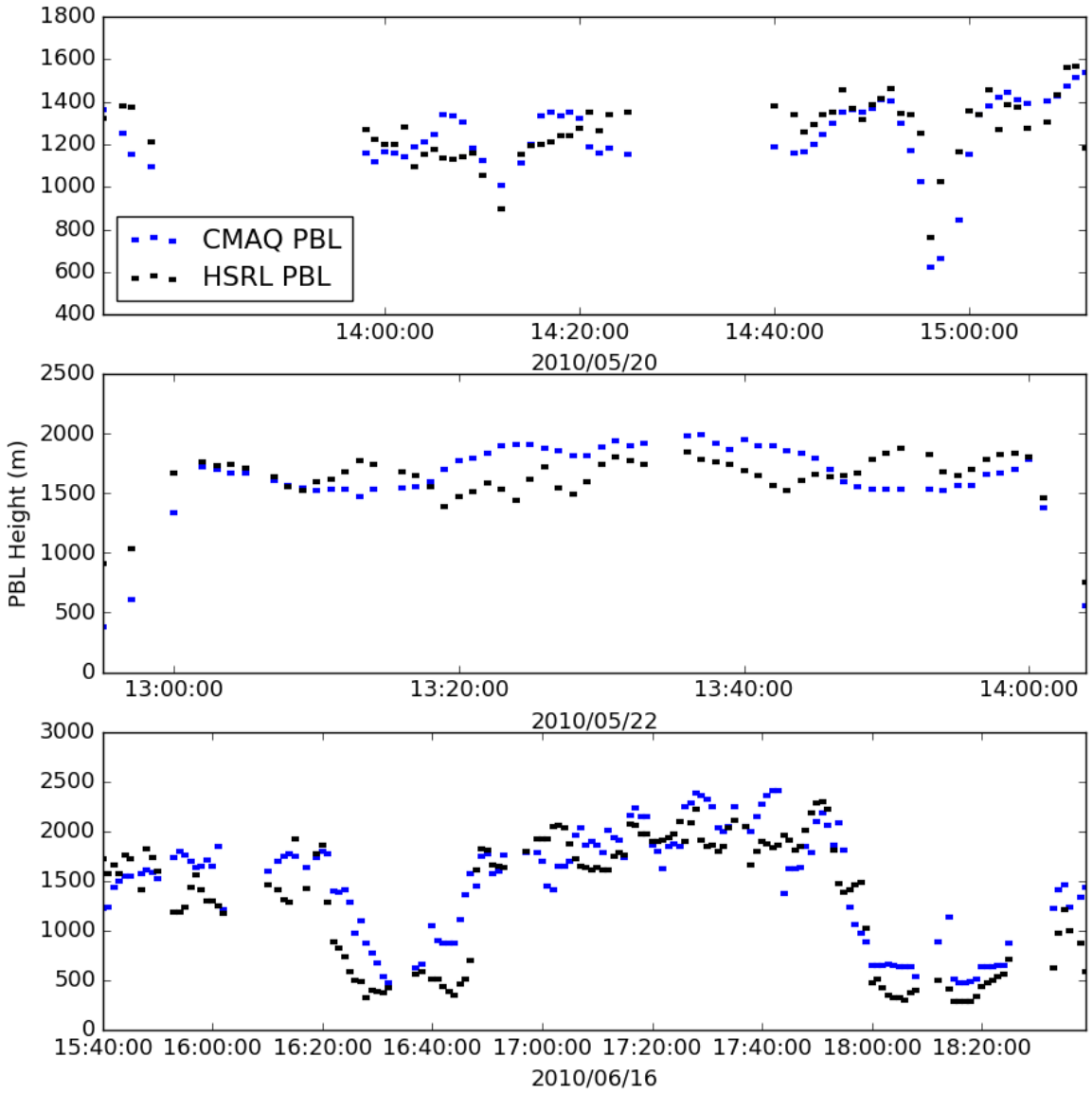

Figure 4. Time series of WRF predicted planetary boundary layer heights and HSRL calculated mixed layer heights for 3 flight sections in the San Joaquin Valley (2 during CalNex and one during a CARES campaign).

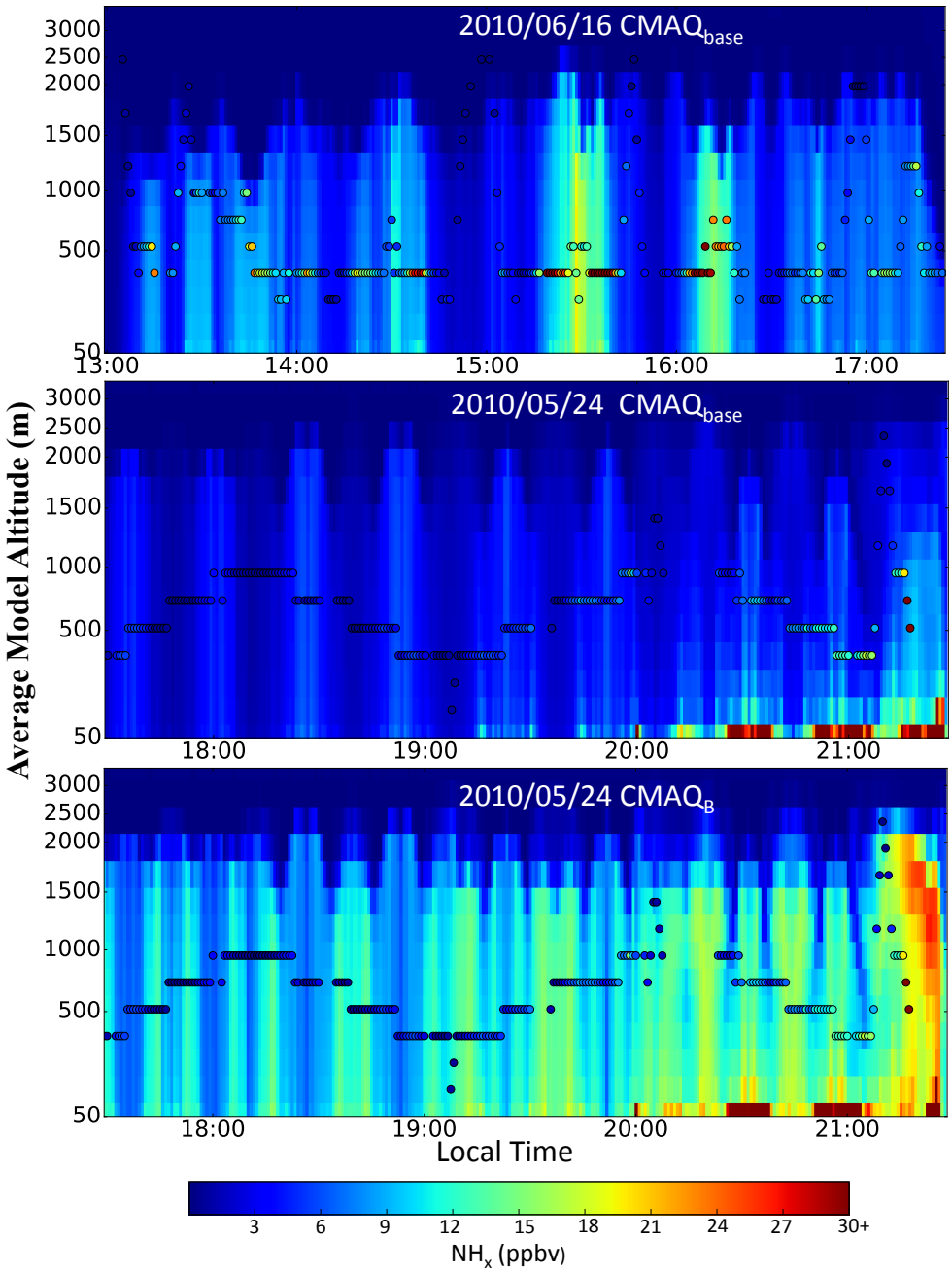

Figure 5. The hourly output of $CMAQ_{base}$ NH_x is shown in the background with the measured (one minute average) NH_x concentrations within the modelled hour shown as the dots. (a) Daytime flight over Bakersfield on June 16, (b) evening flight on May 24, 2010 and (c) the same as (b) but for a $CMAQ_B$ run.

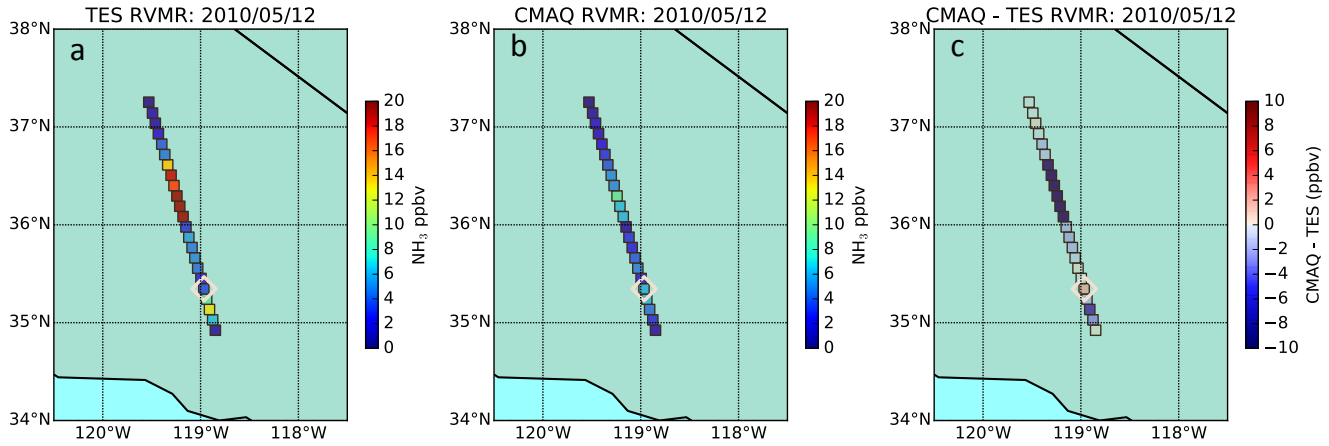

Figure 6. NH_3 representative volume mixing ratios (RVMRs) on 12 May 2010 during the CALNEX campaign for (a) TES special observations, (b) modelled RVMR for CMAQ and (c) the difference between each RVMR near the Bakersfield, CA, surface site with the white diamond locating the Bakersfield measurement site.

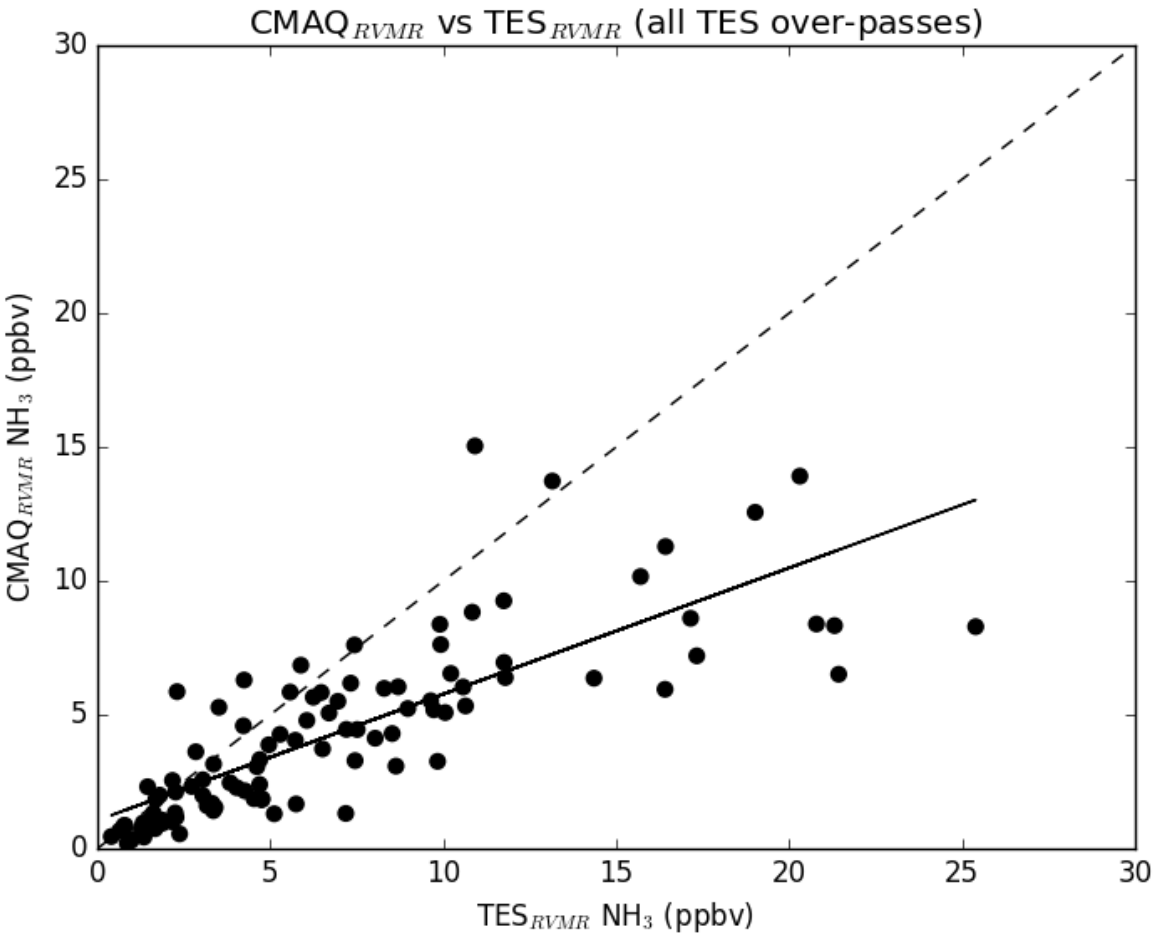

Figure 7. Scatter plot of $CMAQ_{base}$ and TES NH_3 representative volume mixing ratios for four TES special observation passes (TES_{RVMR}) during the CalNex campaign with statistics discussed in Table 3.

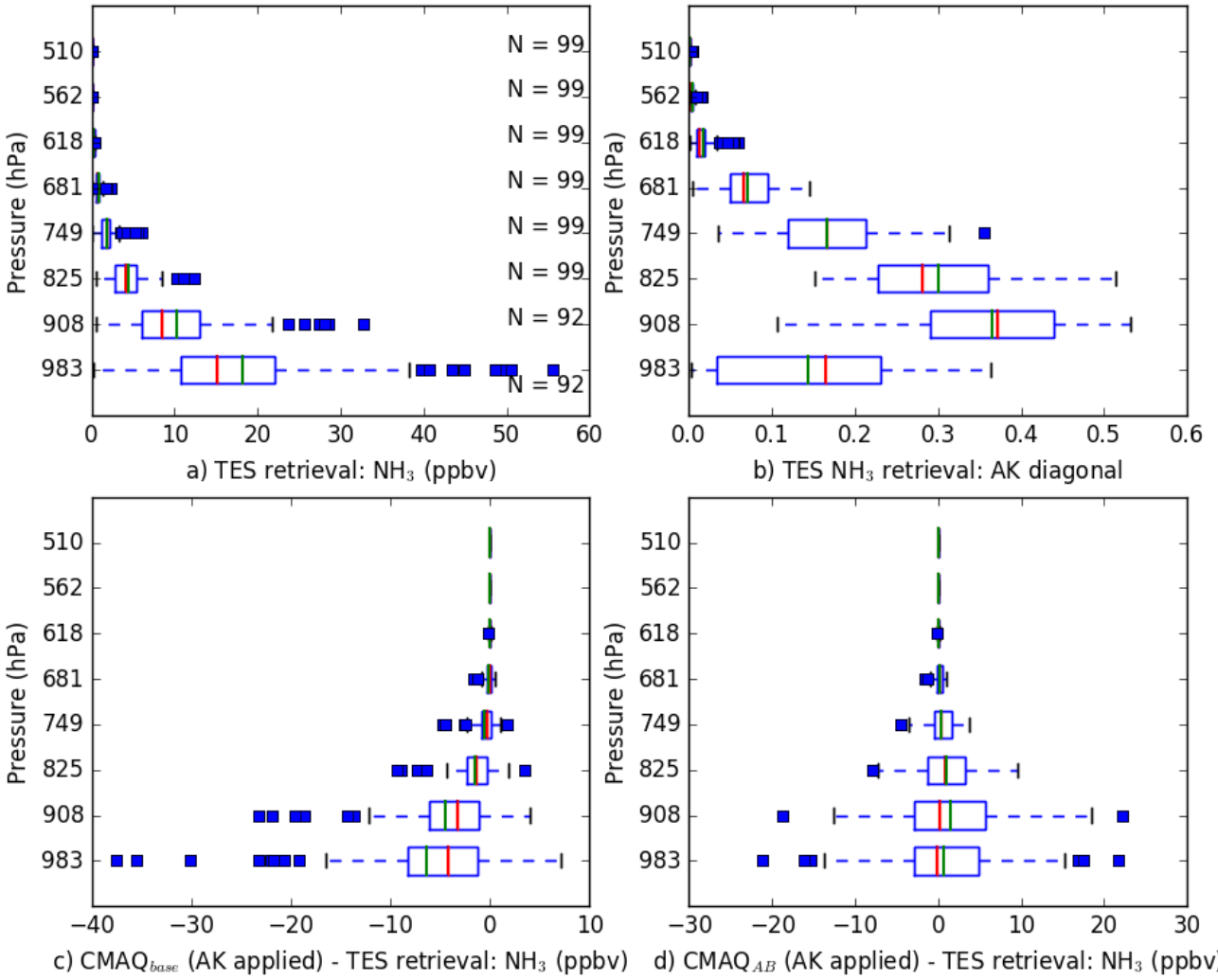

Figure 8. Boxplots of a) TES NH_3 retrieval by pressure level, b) TES NH_3 retrieval averaging kernel (AK) diagonal, c) difference between the TES NH_3 retrieval and $CMAQ_{base}$ modelled NH_3 interpolated to TES levels with an AK applied for the baseline model run and d) same as c) but for the $CMAQ_{AB}$ run. Box plots show the mean (green), median (red), interquartile range (IQR, blue box), whiskers at 1.5 IQR and outliers beyond that.

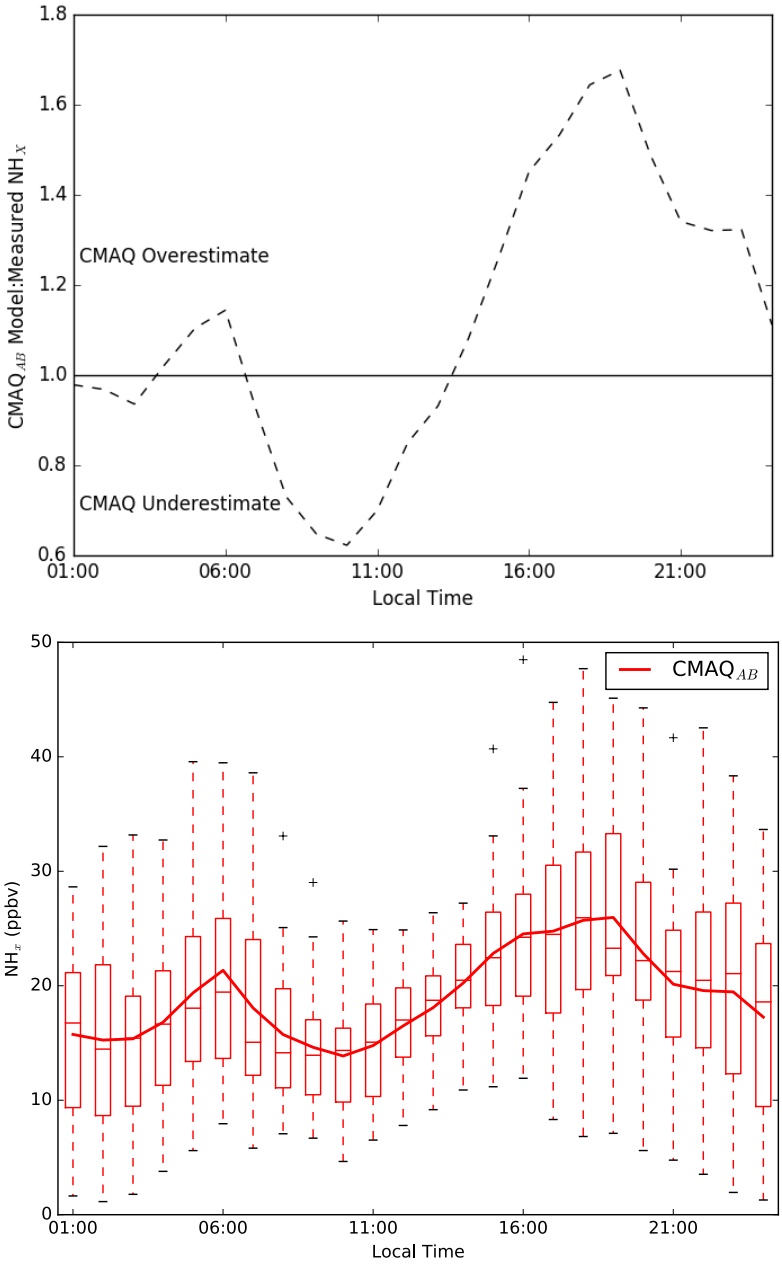

Figure 9. a) The average hourly ratio of $CMAQ_{AB}$ modelled to measured NH_x (dashed line) mixing ratios at the Bakersfield ground site b) Boxplot of average hourly $CMAQ_{AB}$ modelled (red) NH_x mixing ratios for the Bakersfield ground site.